

Wetting and particle adsorption in nano flows

Germán Drazer^{a)} and Boris Khusid^{b)}, Joel Koplik^{a); c)}, and Andreas Acrivos^{a)}

^{a)} Levich Institute, City College of the City University of New York, New York, NY 10031.

^{b)} Department of Mechanical Engineering,

New Jersey Institute of Technology, University Heights, Newark, NJ 07102.

^{c)} Department of Physics, City College of the City University of New York, New York, NY 10031.

(Dated: April 14, 2024)

Abstract

Molecular dynamics simulations are used to study the behavior of closely-*ting* spherical and ellipsoidal particles moving through a fluid-filled cylinder at nanometer scales. The particle, the cylinder wall and the fluid solvent are all treated as atomic systems, and special attention is given to the effects of varying the wetting properties of the fluid. Although the modification of the solid-fluid interaction leads to significant changes in the microstructure of the fluid, its transport properties are found to be the same as in bulk. Independently of the shape and relative size of the particle, we find two distinct regimes as a function of the degree of wetting, with a sharp transition between them. In the case of a highly-wetting suspending fluid, the particle moves through the cylinder with an average axial velocity in agreement with that obtained from the solution of the continuum Stokes equations. In contrast, in the case of less-wetting fluids, only the early-time motion of the particle is consistent with continuum dynamics. At later times, the particle is eventually adsorbed onto the wall and subsequently executes an intermittent stick-slip motion. We show that van der Waals forces are the dominant contribution to the particle adsorption phenomenon and that depletion forces are weak enough to allow, in the highly-wetting situation, an initially adsorbed particle to spontaneously desorb.

PACS numbers: 47.15.Gf, 47.11.+j, 47.15.Rg, 68.08.-p

Keywords: nanochannel, molecular dynamics, suspension

I. INTRODUCTION

The flow of particles of different shapes suspended in Newtonian fluids at low Reynolds numbers and transported through different geometries has already been studied for over a century, and the use of a continuum description through the Stokes equations to model such phenomena has proved extremely successful.¹ There exist, however, situations in which the flow involves characteristic length scales far beyond the range of applicability of the continuum equations of fluid mechanics, and a microscopic, molecular detail of the fluid behavior and that of fluid-solid interfaces, may provide crucial understanding.² A paradigmatic example of this situation refers to the recurring question regarding the appropriate boundary conditions at the fluid-solid and fluid-fluid interfaces, a long standing problem that arises in the description of two immiscible fluids moving along a solid-surface.^{3,4} In recent years, the sustained development of new microfluidic devices and their potential applications in a variety of fields, particularly those associated with the so called lab-on-a-chip⁵ devices or *microfluidics*,^{6,7} have led to a renewed interest in the problem of fluid flow under microscopic confinement.^{8,9,10,11} Moreover, novel fabrication techniques are reaching resolutions in the nanometer scale^{12,13} and nanofluidic devices are beginning to emerge as powerful tools in biotechnology and related areas.¹⁴ One of the fundamental advantages that renders miniaturization so attractive in biotechnology is its potential ability to detect, transport and interrogate single particles at the molecular level. Of exceptional promise are those devices that take advantage of fluid flow and suspension flow behavior only available at the molecular scale. It is clear then that, in order to realize this promise and exploit the potential benefits of such nanodevices, it is crucially important to understand both the transport of nanometer size particles through nanochannels as well as its distinctive physics under nano-confinement. In this context, molecular simulations provide a powerful tool that have been successfully applied to the study of the effects of nanoconfinement in single fluids, and have thereby illustrated a variety of novel and interesting dynamic behavior which drastically differs from the hydrodynamics of bulk fluids.^{15,16,17}

In a previous letter, we investigated by means of Molecular Dynamics (MD) simulations the low Reynolds number motion of a solid sphere in a fluid-filled capillary tube when the dimensions of both the particle and the channel approach the molecular scale.¹⁸ Specifically, we examined the behavior of the system as the wetting properties of the fluid are varied from perfect to partial

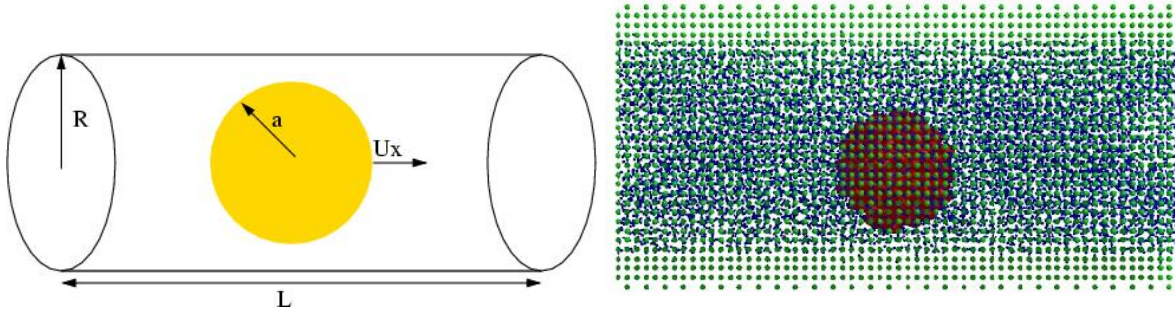


FIG. 1: Schematic and explicit views of a colloidal spherical particle moving in a nanochannel.

wetting, and identified a novel adsorption phenomenon in which, for poorly wetting fluids, a solid sphere, initially moving along the center of the nanochannel, is adsorbed onto the tube wall while displacing all the fluid molecules from the particle-wall gap. Here we present a detailed study of such adsorption phenomena, with particular emphasis on: i) The nature of the transition from adsorption to no-adsorption as the wetting improves, and its dependence on the shape of the particles; ii) The role and relative importance of the depletion and dispersion forces on the adsorption phenomena; iii) The behavior of elongated particles, which exhibit orientational selectivity upon adsorption; iv) The stochastic behavior of the adsorption phenomena, particularly the times at which adsorption takes place, the reversibility of the adsorption process, and the correlation between the stick-slip motion displayed after adsorption and the velocity fluctuations of the particle.

II. MOLECULAR DYNAMICS SIMULATIONS

The numerical calculations are based on standard MD techniques applied to the system shown schematically in Fig. 1, specially, a colloidal particle moving under the action of an external force through a periodic cylindrical channel. The particle, the wall of the channel, and the fluid are all treated as atomic systems interacting via Lennard-Jones (LJ) potentials,

$$V_{LV} = 4 \epsilon \left(\frac{\sigma}{r} \right)^{12} - A \left(\frac{\sigma}{r} \right)^6 : \quad (1)$$

Here r is the interatomic separation, σ is roughly the atomic diameter and will be used as a length scale, ϵ is the depth of the potential well and will be used as an energy scale, and A is an adjustable parameter which controls the attraction between the various atomic species.

Although we consider generic non-polar materials, typically σ is a few Angstroms, $\epsilon = 0.1(10^2 k_B)$, where k_B is Boltzmann's constant, and the intrinsic atomic time scale $\tau = \sqrt{\frac{m}{k}}$ is a few picoseconds.¹⁹ In the remainder of the paper, all quantities are expressed in LJ reduced units using σ , ϵ and τ as characteristic length, energy and time scales, respectively. The potential is truncated at $r_c = 2.5$ and shifted by a linear term so that the force vanishes smoothly at the cutoff. Newton's equations are integrated with a fifth-order predictor-corrector scheme, with a time step $\Delta t = 0.005$. The temperature of the system is $T = 1.0$, which is maintained in the fluid by a Nose-Hoover thermostat with relaxation time²⁰ $Q = 10$, and in the solid by velocity rescaling.

The confining wall is composed of atoms of mass $m_w = 100$, tethered to fixed lattice sites by a stiff linear spring with constant $k_w = 100$. The wall sites are obtained from a cylindrical section of an fcc lattice of length L_x and inner and outer radii R and $R_o = R + 3\sqrt{2}$, respectively. Here $\sqrt{2} = 1.41$ is the fcc lattice constant, corresponding to a wall number density $\rho_w = 0.8$. We refer to this channel as an ordered cylinder, and also consider a disordered version, where the equilibrium position of each atom is perturbed by a random displacement in each direction, uniformly distributed in the range $-\sqrt{6} < \Delta r < \sqrt{6}$.

The spherical nanoparticle is constructed in an analogous fashion, from lattice sites lying within a spherical volume of radius $a = 3\sqrt{2} = 4.24$. Again we consider both ordered and disordered spheres, where in the latter case the atomic positions are perturbed randomly as is done for the wall, with $-\sqrt{5} < \Delta r < \sqrt{5}$. The atoms in the particle are however fixed at the lattice sites, allowing the motion of the nanoparticle to be computed by rigid body dynamics. The total force and torque on the particle are found by summing the individual atomic forces acting on all of its atoms, and Newton's and Euler's equations are integrated to give the particle's motion.²¹ We assume here that the particle and channel wall are made of the same material and that their atoms interact via the LJ potential with $A = 1$.

The fluid atoms are initialized on fcc lattice sites with the same average density as the wall, interacting among themselves with the $A = 1$ standard LJ potential. The volume-average number density of the fluid is the same as that of the tube wall, $\rho_{av} = 0.8$, which, at $T = 1.0$, corresponds to the fluid phase of the Lennard-Jones bulk system, slightly above the critical temperature,²² $T_c = 0.937$. The fluid is allowed to "melt" off the original lattice sites for a few using velocity rescaling, and then is equilibrated using the Nose-Hoover thermostat. A typical system has

length $L_x = 20' = 34.20$, inner radius $R = 12' = 20.52$, outer radius $R_o = 13.5' = 23.09$. and contains 35860 fluid atoms, 459 atoms inside the nanoparticle, and 9920 solid molecules in the tube wall. Figure 1 shows a snapshot of all atoms after equilibration.

A key feature in these simulations is the interaction between the fluid and the solid atoms, specified by the parameter A in Eq. (1), which provides a simple means of controlling the wetting properties of the fluid-solid system. Recent simulations using similar parameters showed that varying A from 1.0 to 0.5 leads to a transition from wetting to nonwetting behavior for a liquid drop on a solid substrate.^{23,24} Moreover, a common approximation for the contact angle in LJ systems, based on Young's law and a Laplace estimate for the surface energies,^{25,26} is $\cos(\theta) =$

$1 + 2A$. In our simulations, we vary A from 0 to 1, corresponding to estimated contact angles ranging from π to 0. A second interpretation of A arises from MD simulations of dilute gas flow in the Knudsen regime, where²⁷ $A = 1$ corresponds to an ideal thermal wall in which a molecule, colliding with the solid, undergoes a diffusive collision and emerges from the wall with an uncorrelated random velocity, distributed according to a Maxwell distribution at the temperature of the wall. The opposite limit, $A = 0$, corresponds to specular reflection where the normal velocity is reversed while the tangential component is preserved.

III. FLOW OF A SINGLE FLUID THROUGH A CYLINDRICAL NANOCHANNEL

The confinement of fluids at nanometer scales has a major impact on their rheological behavior, mainly due to the increasing influence of the interfaces as the surface-to-volume ratio is increased. We shall show, for example, that a variation in the solid-fluid interaction, which induces an order of magnitude displacement in the location of the first peak of the fluid density profile adjacent to the wall (the position of the first fluid layer that is adsorbed onto the wall, see Fig. 2) leads to noticeable changes in the average density at the center of the tube, in contrast to macroscopic flows. In turn, these small but noticeable changes in density induce substantial changes in the fluid viscosity. Thus, it is important to characterize first the behavior of single fluid flows in nanochannels under different wetting conditions, to provide some necessary background for the nanoparticle simulations. We begin, therefore, by discussing how the flow characteristics of the pure fluid vary with channel radius and wetting behavior. We consider Poiseuille flow, in the ordered-wall case, which is generated by applying to each fluid atom a body force f in the axial direction. After

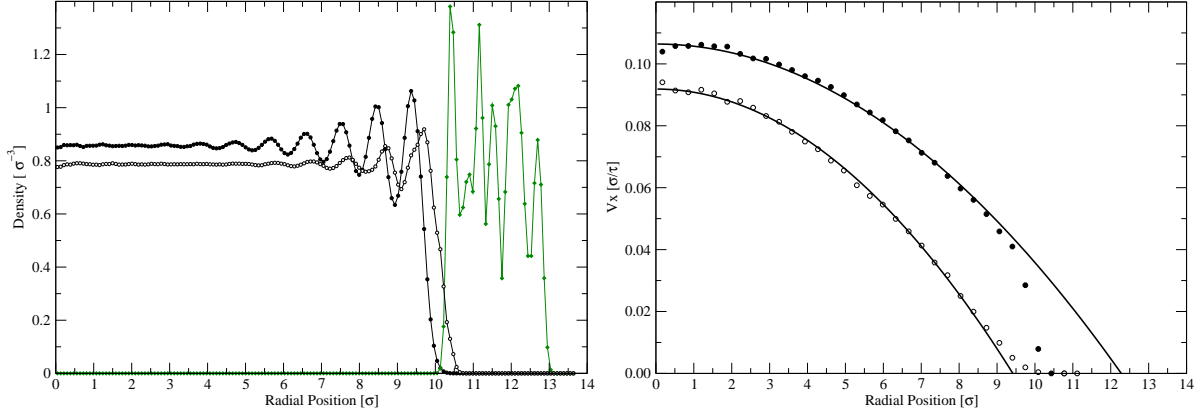


FIG. 2: Pure fluid profiles for channel radius $R = 6 \text{ Å} = 10.26$; open and solid circles correspond to $A = 1.0$ and $A = 0.1$, respectively. The data points are obtained as histograms by dividing the interior of the tube into cylindrical shells of thickness $0.05 \text{ Å} = 0.0855$. (a) Density vs. r ; the curves are drawn through the data points to guide the eye. (b) Axial velocity vs. r ; the curves are best fits to a parabolic profile.

an equilibration period of 5 ns, this force is linearly ramped up from zero over 50 ns, and then held constant at $f = 0.01$ for 500 ns while the time-averaged density and velocity profiles are measured. We average over five realizations each for three values of tube (inner) radius, $R = (4; 6; 12) \text{ Å}$. The qualitative features of the results are the same for each radius, although the differences in detail merit discussion, so we show the profiles for the intermediate case in Fig. 2 and some numerical results in Figs. 2-4, and Table I. For $R = 12 \text{ Å}$ and $A = 0.1$, the average fluid velocity is $v_x = 0.3$ and thus the Reynolds number is $Re = 2$, which is therefore the largest Reynolds number in our simulations.

The density profiles show a wall-induced layering similar to that observed in liquids confined between planar surfaces, in both experiments²⁸ and MD simulations,^{29,30} and also predicted theoretically for the case of hard-sphere systems.³¹ It is important to note that we have also performed equilibrium simulations in the absence of flow and found that the density profile agreed exactly, within the available sensitivity of the numerical simulations, with the non-equilibrium profiles obtained in the presence of flow. It is impressive that a system driven so far from equilibrium by extremely large shear rates, 10^0 s^{-1} , has the same statistical structure at the microscopic level (singlet distribution function) as the system in thermodynamic equilibrium.³² In most cases the density reaches a constant well-defined value at the center of the tube, although

its magnitude differs from the volume-average density $\rho_{av} = 0.8$, a consequence of the attraction or repulsion of fluid atoms near the wall. But, when $A = 1.0$, in all cases the density at the center remains essentially equal to 0.8, reflecting the fact that the fluid and solid have the same density and that their atoms have the same interactions. On the other hand, since, even for $A = 1.0$, there exists still a layer of fluid adsorbed at the wall which slightly depletes atoms from the bulk, the density at the center is reduced, as seen in Table I. The number of noticeable layers at $A = 1.0$ is 5-6. In contrast, in simulations with poor wetting, $A = 0.1$, the fluid avoids the wall and the first liquid layer is displaced towards the tube center, resulting in an obvious increase in the fluid density at the center. A larger number of layers is observed in this case, 6-7, probably due to the higher packing as a result of the same wall-repulsion effect, and, for the smallest systems, the density oscillations persist all the way to the center of the channel.

The velocity profiles in Fig. 2 (and in the other cases not displayed) are also similar to those observed in LJ fluids confined between planar surfaces.^{30,36} Except for the region near the wall, the data are accurately fitted by a parabolic profile $v_x(r) = c_1 - c_2 r^2$, from which we can obtain an effective viscosity $\eta = \tau/4c_2$ (Note that this way of computing the effective viscosity is different from the more standard calculation in which the stress tensor is computed in a simple shear flow³). In addition, a slip length can be defined either as the distance from the wall where the fitted velocity extrapolates to zero, $l_1 = (c_1/c_2)^{1/2} R$, or through a Navier condition relating the fluid velocity v_s and the shear stress τ_s at the surface, $v_s = l_2 \tau_s$, which gives $l_2 = [v_x = (dv_x/dr)]_k = (c_1 - c_2 R^2)/(2c_2 R)$. The two estimates of the slip length agree, as seen in Table I and in Fig. 4. As was said earlier, in the $A = 1$ wetting case, there is little variation in the fluid density at the center of the tube, hence only small variations in the fluid viscosity are observed, with mean values ranging from $\eta = 1.83$ for $R = 4$ to $\eta = 2.05$ for $R = 12$. On the other hand, larger variations in the central density for the non-wetting $A = 0.1$ situation lead to even larger variations in the measured viscosity, which now varies from $\eta = 3.3$ for $R = 4$ to $\eta = 2.63 \pm 0.01$ for $R = 12$. However, in all cases, the viscosity variation correlates closely with the density variation, and agrees with previously reported experimental and numerical results for the shear viscosity of liquid Argon, as shown in Fig. 3. The slip length remains constant and negative for all tube sizes in the wetting simulations, $l_1 = -2$, due to the locking of the first layer next to the solid surface, and again is in complete agreement with previously reported results in planar geometries.³⁶ The non-wetting case $A = 0.1$ shows larger slip at the fluid-solid interface,

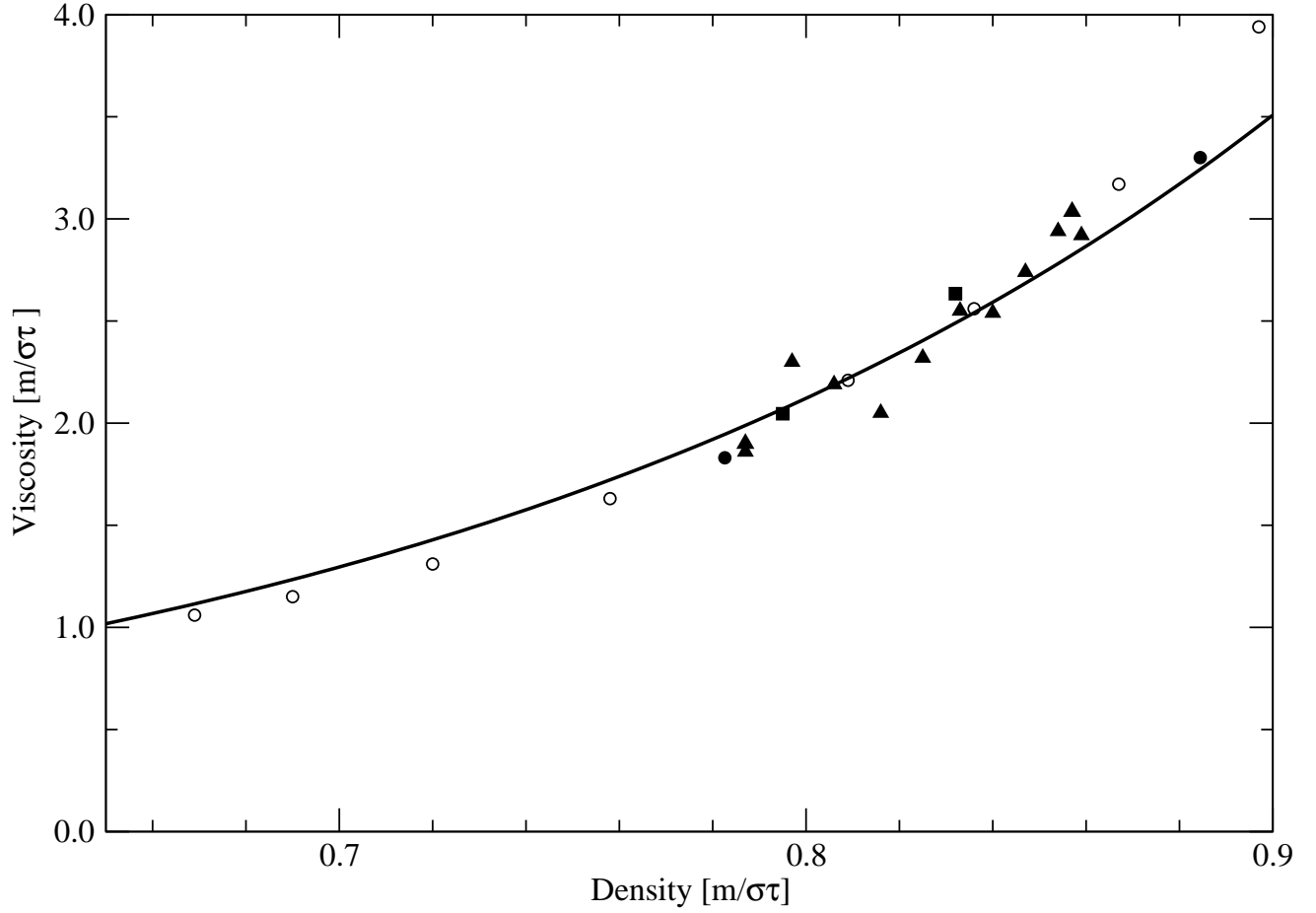


FIG .3: Shear viscosity for the Lennard-Jones fluid as a function of the central density. The solid circles, triangles and squares are the simulation results listed in Table I for $R = 4, 6$ and 12 , respectively. The open circles are published numerical results for the shear viscosity of LJ bulk system s ,³³ and the solid line is an empirical fit to the experimental shear-viscosity data for Argon,³⁴ $\eta(\rho) = \eta_0 + 0.0324(\exp(5.18(\rho - \rho_0)))$, where η_0 is the dilute-gas value limit of the viscosity at³⁵ $T = 1$.

as can be seen in the velocity profiles, since the fluid is no longer locked to the wall,³⁷ but the slip length is still $O(\epsilon)$, also in agreement with previous results obtained in planar Couette and Poiseuille flows with similar fluid densities.³⁶

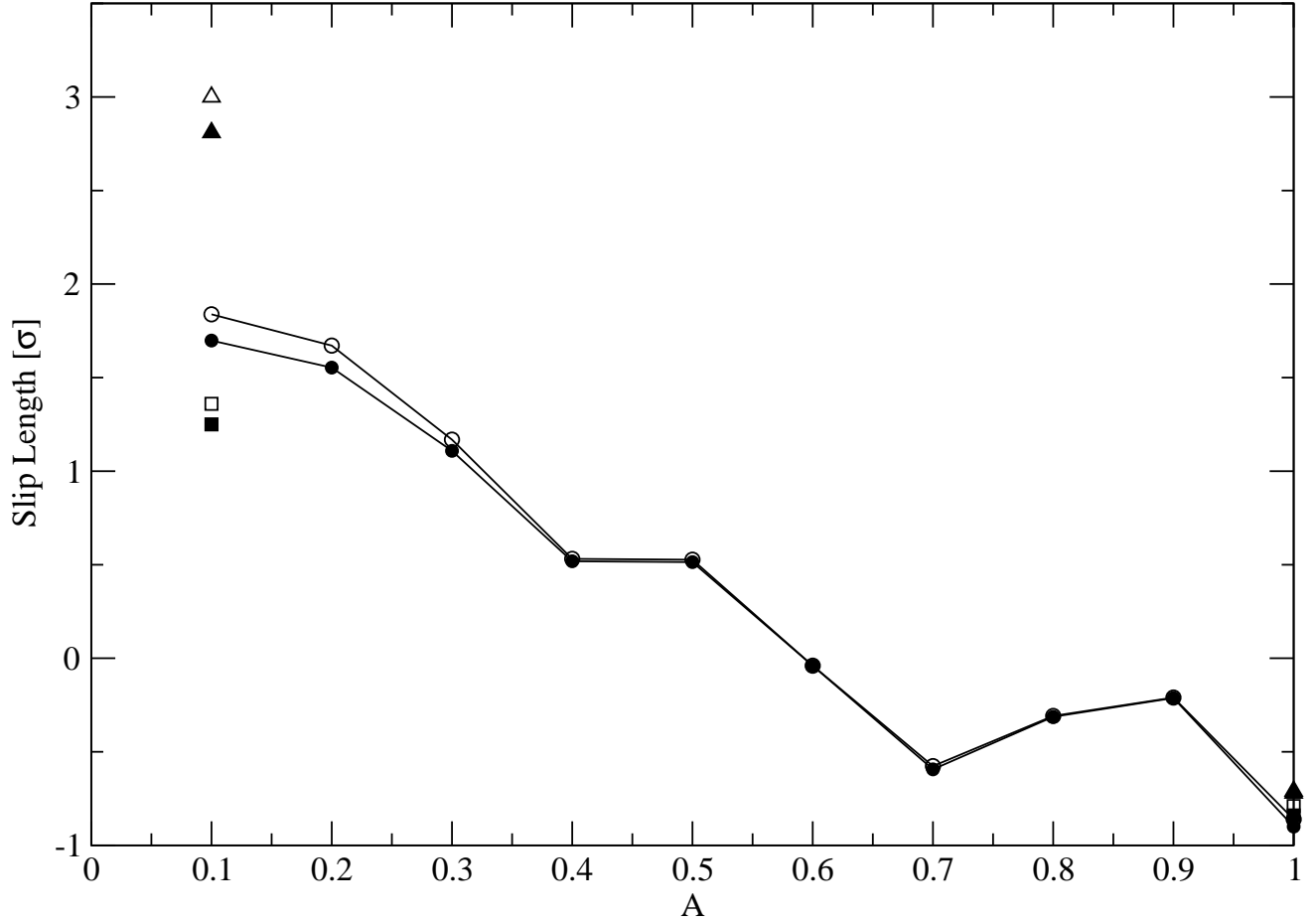


FIG. 4: Slip length for the Poiseuille flow in a narrow tube as a function of the wetting parameter A . The solid (open) squares, circles and triangles correspond to simulation results for the slip length l_1 (l_2) in tubes of radius $R = 4, 6$ and 12 \AA , respectively.

IV. MOTION OF A SPHERE THROUGH A CYLINDRICAL NANOCHANNEL: SHORT TIMES

We now consider the motion of a spherical solid particle forced through a cylindrical tube of nanometer dimensions. As discussed in our previous work,¹⁸ the motion of the suspended Brownian particle, initially located in the middle of the tube, can be divided into two different regimes. The first occurs at early times, for which the particle has not deviated substantially from its centerline motion and, thus, does not directly interact with the tube wall. This initial regime was shown to be amenable of a continuum description. The second regime corresponds to the long time behavior of the particle, after the diffusive motion has allowed it to sample the

TABLE I: Numerical results for pure uid ow. Average central density, Poiseuille tting results, viscosity and slip lengths.

$R = \lambda$	A	$\rho(0)$	η	λ_1	λ_2
4	1.0	0.783	1.83	-0.79	-0.84
	0.1	0.884	3.30	1.36	1.25
6	1.0	0.787	1.86	-0.86	-0.90
	0.9	0.797	2.30	-0.21	-0.21
	0.8	0.806	2.19	-0.31	-0.31
	0.7	0.816	2.05	-0.57	-0.59
	0.6	0.825	2.32	-0.04	-0.04
	0.5	0.833	2.55	0.53	0.52
	0.4	0.840	2.54	0.53	0.52
	0.3	0.847	2.74	1.17	1.11
	0.2	0.854	2.94	1.55	1.67
	0.1	0.859	2.92	1.70	1.84
12	1.0	0.794	2.05	-0.71	-0.72
	0.1	0.832	2.63	3.00	2.81

accessible cross section. In this section we shall examine the behavior at early times and focus on the particle's mobility. The ordered spherical particle of radius $a = 3\lambda = 5.13$ is initially located at the center of the tube and is allowed to equilibrate with the uid for 10^4 , whereupon a body force is ramped up from zero to $f = 0.1$ over a 40^4 interval. We performed simulations for tube radii ranging from $R = 4\lambda$ to $R = 14\lambda$, corresponding to relative sizes $4/3 < R/a < 14/3$, and for a length of the (ordered) tube $L_x = 30\lambda$.

Periodic boundary conditions are used in the axial direction, implying that the simulations in fact correspond to the motion of the "real" sphere and an infinite string of periodic replicas. Since hydrodynamic interactions between suspended solid particles are usually long-ranged, one might be concerned about the interactions between the periodic images. Fortunately, however, confining geometries effectively screen such hydrodynamic interactions and lead to a much faster spatial decay of the disturbances created by a single particle, typically exponentially with a characteristic

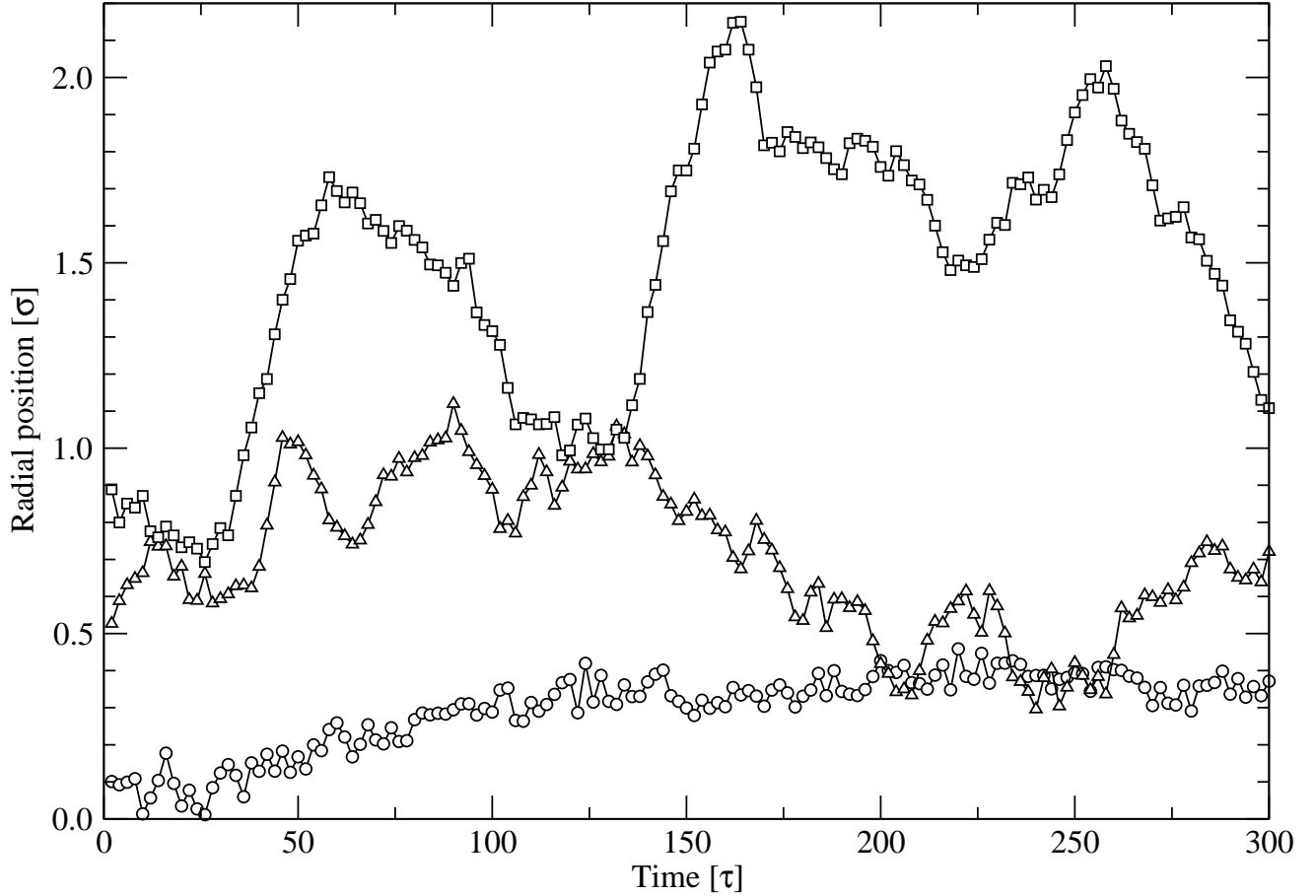


FIG. 5: Radial position of the spherical particle, $a = 3$, as a function of time for tube radii $R = 4$ (open circles), $R = 6$ (open triangles) and $R = 14$ (open squares). Time $t = 0$ corresponds to end of the force ramp. In all cases there is perfect wetting, $A = 1.0$.

length fixed by the tube radius³⁸ R . In particular, the interaction between spheres, equally spaced along the centerline of a tube, has been shown to be small when the separation between spheres is larger than one tube diameter,³⁹ and recent experiments involving colloidal particles in a narrow channel have demonstrated that hydrodynamic interactions are indeed strongly inhibited by the one-dimensional confinement.⁴⁰ Given that, even in the worst scenario, we have $L_x = R > 2$, we can then safely neglect any hydrodynamic interactions with the periodic copies of the particle.

The radial motion at short times is indicated in Fig. 5, for $A = 1.0$ and for three different values of the tube radius. The motion is roughly random and diffusive, but its range in the radial direction is constrained by the presence of the tube, decreasing as the tube radius approaches that of the particle. To examine the axial velocity, we follow the evolution of the particle for

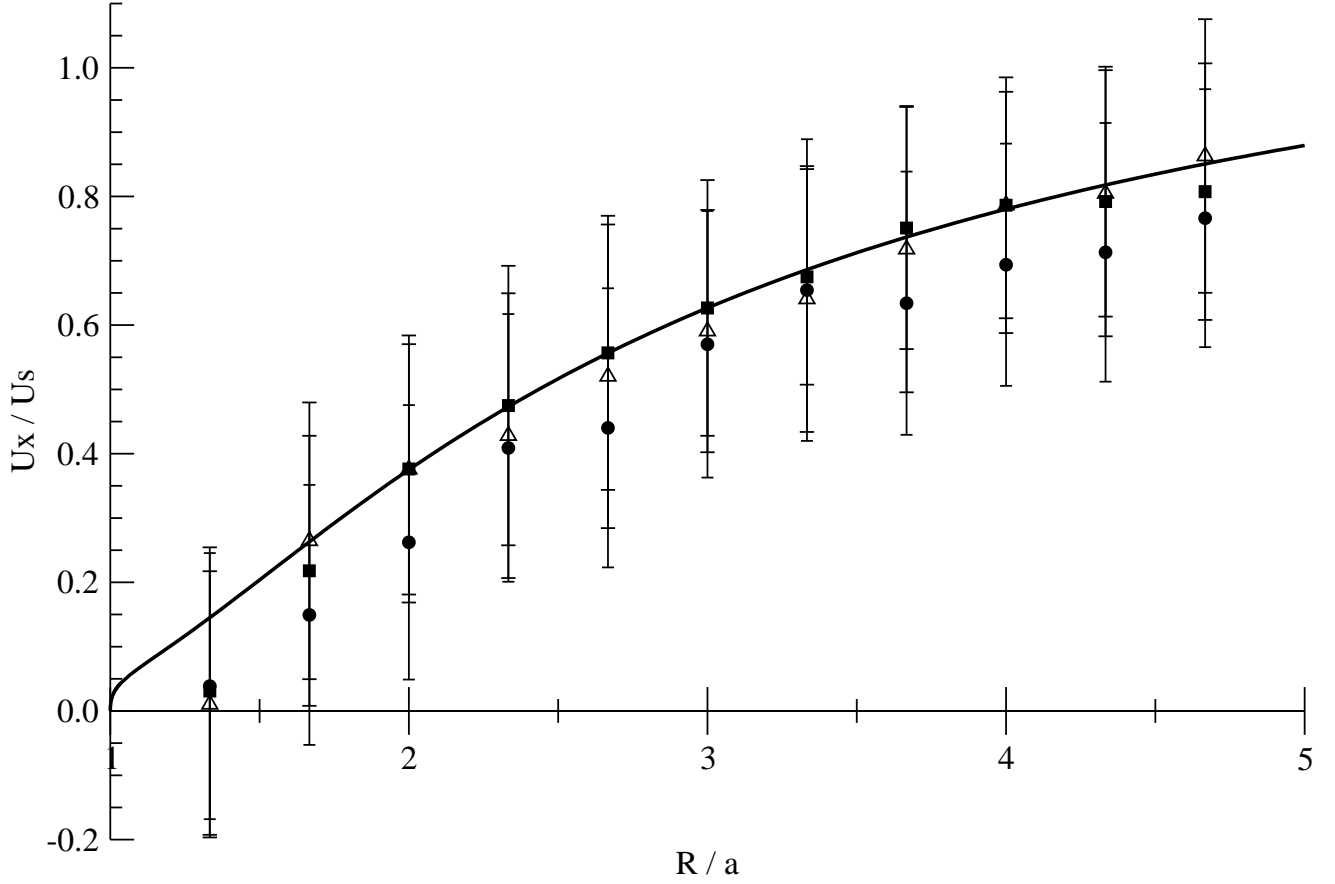


FIG . 6: Particle average axial velocity, normalized by the Stokes velocity U_s ($\eta_{av} = 1.94$; $N_a = 438$), as a function of the relative size of the tube radius: $A = 1.0$ (closed circles), $A = 0.5$ (open triangles) and $A = 0.25$ (closed squares). The solid curve is the theoretical prediction of Ref. 41, as discussed in the text.

300, measuring the velocity every 2 and averaging the last 100 points (corresponding to a time average over about half a nanosecond). In Fig. 6 we present the average axial velocity of the sphere, U_x , as a function of the relative size of the tube R/a . Note the large error bars in the figure which reflect the substantial fluctuations in the velocity of the particle due to the thermal motion. The axial velocity is normalized by the Stokes velocity, the velocity which the particle would have had in an unbounded fluid under the action of the same external body force, $U_s = F/(6\pi\eta a)$, where $F = N_a f$ is the total force acting on the particle and N_a the total number of atoms in it. Using the measured average viscosity as described in Section III, $\eta_{av} = 1.94$, and the average number of atoms in a spherical particle, $N_a = 438$, we obtain $U_s = 0.23$. (A similar

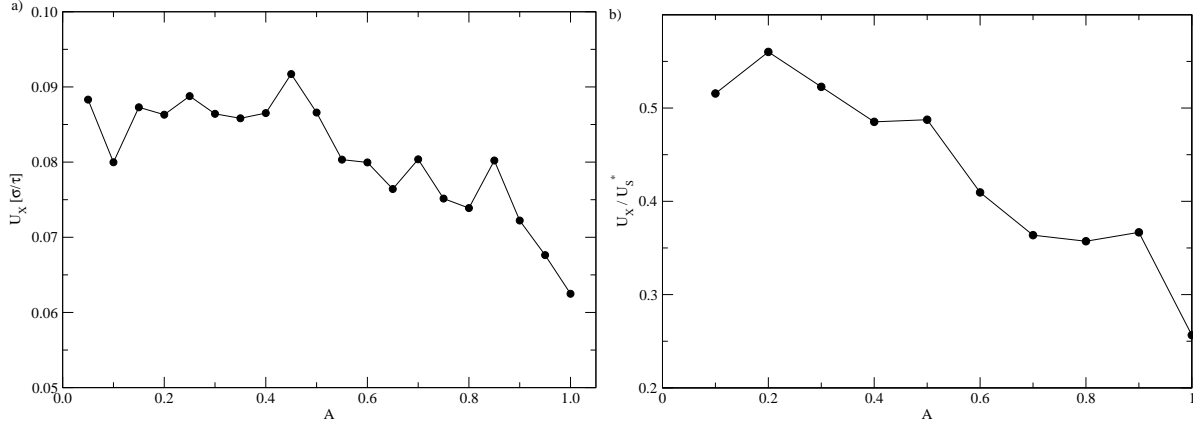


FIG. 7: Particle average axial velocity as a function of the wetting properties of the system (The tube radius is $R = 6 \text{ \AA}$ and the particle radius is $a = 3 \text{ \AA}$). (a) The velocity is given in MD units. (b) The velocity is normalized by a Stokes velocity U_s^* that accounts for the variations in the viscosity, $U_s^* = F/(6\eta a)$, with η being the viscosity values listed in Table I.

value, $U_s = 0.22$, is obtained using the experimental value of the viscosity at the volume-average density and the average force on a sphere with the same density). There is some ambiguity in the Stokes velocity arising from an ambiguity in the particle radius in that, if instead of taking the radius of the suspended particle as $a = 5.13$, we were to define the effective hydrodynamic radius as that of the volume inaccessible to the fluid molecules,⁴² $a_e = a + 1$, the predicted Stokes velocity would decrease by about 20%. This uncertainty in the definition of the particle radius is intrinsic to its molecular nature and the small length scales involved in the problem. Also note that the Stokes velocity, $U_s = 0.23$, was computed using the average viscosity obtained for $A = 1.0$ and it does not account for the variations in the viscosity that occur due to changes in the wetting properties (see Fig. 3). As shown in Fig. 7 (a), there is little statistically significant variation of the velocities with changes in the wetting parameter A , particularly below about $A = 0.5$. On the other hand, when the velocity is normalized by a Stokes velocity that accounts for the variations in the viscosity, $U_s^* = F/(6\eta a)$, with η being the viscosity values listed in Table I, a completely different picture emerges, as can be observed in Fig. 7 (b), showing a systematic increase in the velocity with decreasing A . We can then conclude that the apparent lack of dependence of the average velocity on the wetting properties, observed in Fig. 7 (a), is in fact due to the competition between an increase in the fluid viscosity and a reduction in the drag coefficient of the particles as A is decreased.

Next, we wish to test the degree to which these results can be described by continuum hydrodynamics. Previous studies have shown good agreement in a number of situations,² including the Stokes drag on a sphere in an unbounded fluid,⁴³ even where the particle size is comparable to that of the liquid molecules, and the motion of a spherical particle through a cylindrical pore⁴⁴ where the tube and particle have molecular structure and dimensions similar to those in the present work. (Unfortunately, the particle's axial mobility was not considered in Ref.44.) The particle's radial Brownian motion and molecular-scale surface roughness are difficult to address in standard continuum calculations, so we compare our results with the solution of the Stokes equations for a non-Brownian smooth sphere moving along the center of a smooth tube. Note that although the particle Reynolds number is $Re = 0.5$, computed using the Stokes velocity of the particle in an unbounded fluid, inertia effects will not be accounted for in the continuum calculation. The continuum description we used also neglects density variations across the tube, and the associated viscosity variation discussed in Section III. It is also assumed that the no-slip boundary condition applies at both solid-fluid boundaries and thus we expect this continuum description to more accurately describe the case $A = 1.0$ for which slip effects were shown earlier to be negligible in the pure fluid problem in accordance with previous studies.^{42,43}

The velocity of the particle is determined only in part by the force applied to it, since one must also specify some additional information about the motion of the fluid, such as the pressure drop along the channel, P , or the mean fluid velocity along the tube, v_x . Actually, it is convenient to work with the excess pressure drop due to the presence of the sphere, $P_s = P - P_0$, where $P_0 = 8 L_x v_x / R^2$ is the Poiseuille pressure drop for the pure fluid. The linearity of the Stokes equations and the no-slip boundary condition imply that

$$\frac{F}{(R^2) P_s} = \frac{a^4 R_{FU} R_{FV}}{R_{PU} R_{PV}} \frac{U_x}{v_x} \quad (2)$$

where the resistance matrix elements R are functions of R/a alone when the particle moves along the center of the tube, and were given explicitly by Bungay and Brenner.^{41,45}

In the case at hand, we have periodic boundary conditions in the x direction and the total pressure drop is zero. Therefore $(R^2) P_s = -(R^2) P_0 = -(a) R_0 v_x$, where $R_0 = 8 L_x / a$. Equation (2) can be solved for F and v_x in terms of U_x , and in particular $F = (a) R U_x$ where

$$R = R_{FU} \frac{R_{FV} R_{PU}}{R_0 + R_{PV}} : \quad (3)$$

In Fig. 6 we compare the velocity, as predicted by the above expression, to the numerical results, and see that the agreement is satisfactory, given the substantial error bars (due to thermal fluctuations). Surprisingly, the numerical results are not sensitive to variations in the wetting properties of the system, with a lack of apparent trend in the average velocity as A is decreased from $A = 1.0$ to $A = 0.25$, and the continuum approximations seem to describe all possible wetting conditions. However, note that, by normalizing the particle velocity by a single Stokes velocity, which was computed using the average viscosity η_{av} obtained for $A = 1.0$, we have not eliminated the dependence on A . In particular, its dependence on the wetting parameter A is not accounted for in U_s . Thus, we can conclude again that, owing to the competition between an increase in the viscosity as A is decreased, and the concurrent reduction of the drag on the particles due to a larger slip-effect, the results are strikingly insensitive to variations in the wetting properties of the fluid.

One can show, from Eq. (3) and the explicit forms of the resistance matrix elements given in Ref. 41, that the continuum mobility vanishes as $(1 - R/a)^{1/2}$ as $a \rightarrow R$, but, although this behavior is consistent with the simulations, it does not appear to capture the trend. Indeed, when the gap between the particle and the wall approaches a molecular diameter, one might expect a continuum result to fail, but we do not have precise enough statistics to make a definitive statement.

V. MOTION OF A SPHERE THROUGH A CYLINDRICAL NANOCANNEL: LONG TIMES

The results presented thus far for the mobility of the particle correspond to relatively short-time motions, essentially at the center of the channel, where any direct interactions with the wall can be ignored. After a sufficiently long time, however, the thermal motion of the particle should cause it to sample the whole cross-section so that direct interactions with the tube wall are unavoidable. An estimate of the (diffusive) time required to reach the wall is $\tau_D \approx (R - a)^2/2D$, where the diffusion coefficient in turn can be estimated from its bulk value given by the Stokes-Einstein formula, $D_{bulk} = k_B T/6\pi\eta a$. We find $\tau_D \approx 2500$, roughly 10 times the elapsed time in the simulations described earlier. Therefore, in order to explore wall interactions, we have conducted rather longer simulations, $O(10^4)$, in a channel of radius $R = 2a$ for a range of values

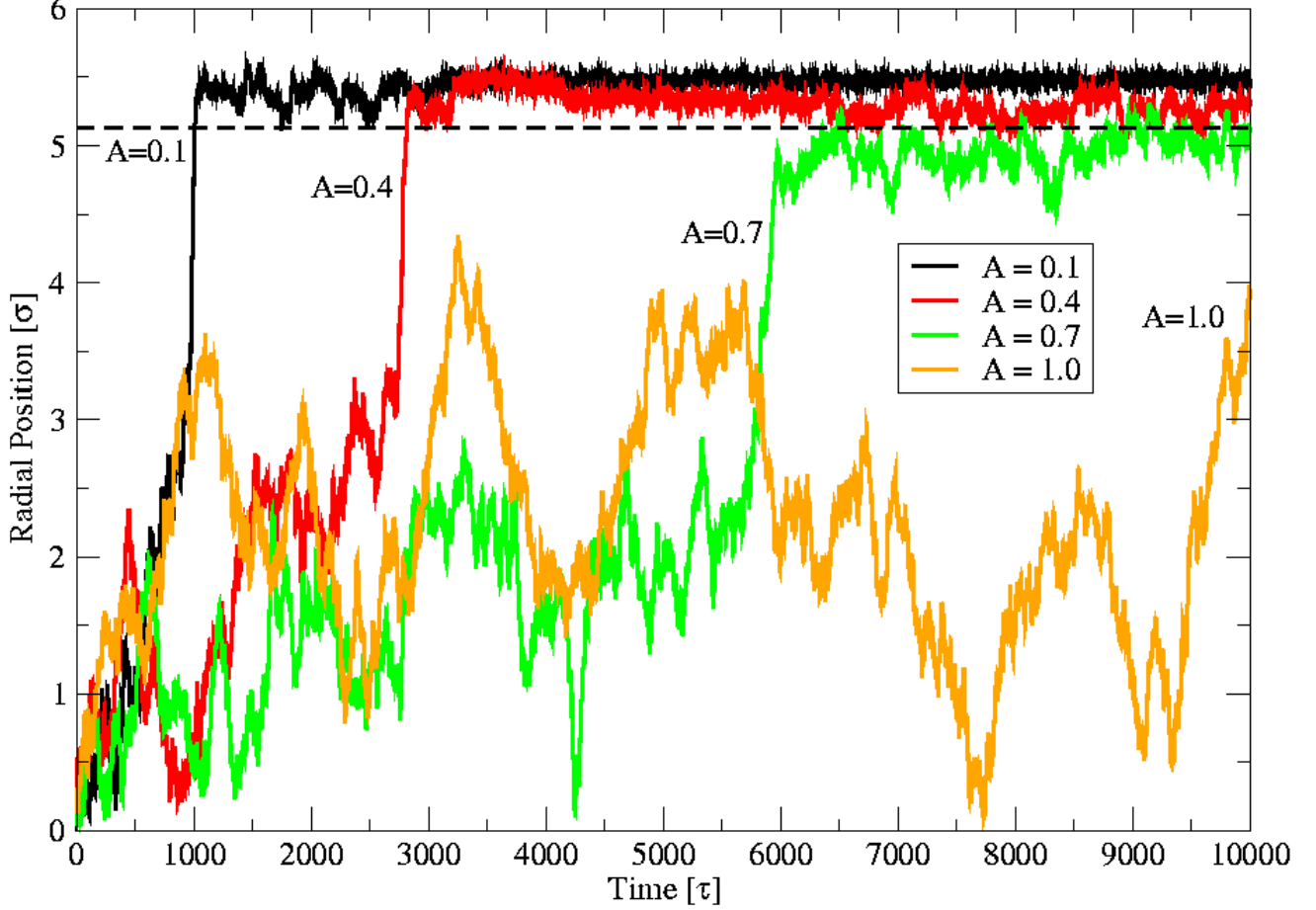


FIG. 8: Radial position of the sphere vs. time for a single realization at four values of A : 0.1, 0.4, 0.7 and 1.0. The sudden jump to a radial position 5 at the three lower values of A corresponds to adsorption at the tube wall. (The tube radius is $R = 6\sigma$ and the particle radius is $a = 3\sigma$. The dashed line corresponds to a radial position equal to $R - a$, the nominal maximum radius.)

of A , for a disordered particle and wall.

Figure 8 illustrates the effects of the wall interaction, showing the radial position of the particle as a function of time for four independent realizations in which the fluid changes from non-wetting to wetting, corresponding to $A = 0.1, 0.4, 0.7$ and 1.0 . The other parameters of the simulation are held fixed: $R = 6\sigma$; $a = 3\sigma$, $L_x = 30\sigma$ and $f = 0.1$. It is seen that, except for the completely wetting case, the particle eventually reaches a critical distance from the wall, and then rapidly moves to the wall and becomes adsorbed, with the adsorption time decreasing with A . Note that, because the sphere and the tube are disordered and the LJ interaction is soft, a particle can reach a radial position with its center located beyond the nominal maximum

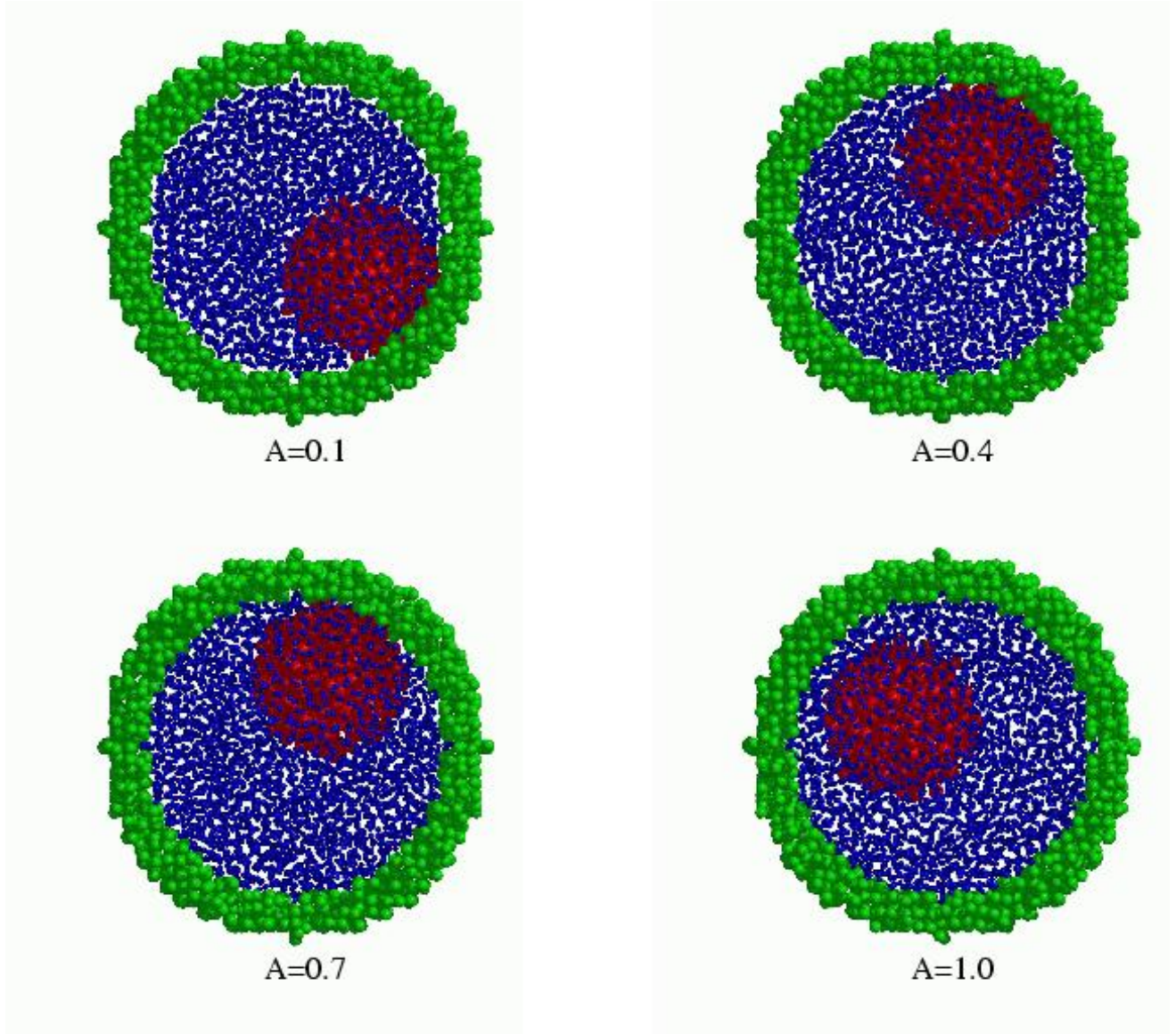


FIG . 9: Cross-section snapshots of the particles at the end of the simulations in Fig. 8. For visual clarity, we use circles of different sizes to represent the different species, with radii in the ratio 1.0 to 0.8 to 0.4 for the particle, wall and fluid atoms, respectively. (The tube radius is $R = 6 \text{ \AA}$ and the particle radius is $a = 3 \text{ \AA}$.)

value $R/a = 5.13$. The snapshots of the final configuration in the simulations in Fig. 9 show that the adsorbed particles are in direct contact with the wall, having expelled the fluid from the gap between them, except for the completely wetting case where an intervening fluid layer persists. To be sure, in any continuum description to this problem, a lubrication force resisting

the particle motion would be generated which would diverge as the gap between particle and wall vanishes.¹ As in earlier MD calculations, however, this divergence cuts off at molecular distances, and in fact the resistance force vanishes when all of the fluid drains out of the gap.⁴³

We can obtain some insight into the particle adsorption by considering the problem in terms of van der Waals interactions between solids, represented by the attraction term of the LJ potential $\phi_{\text{LJ}} = \epsilon \left(\left(\frac{r}{\sigma} \right)^{12} - \left(\frac{r}{\sigma} \right)^6 \right)$. In a continuum description, the attraction energy between a solid wall and a solid sphere of radius R , separated by an empty narrow gap of thickness $h \ll R$, is given by^{31,46,47}

$$V_{\text{sw}}(h) = -A_{\text{H}} \frac{a}{6h} \left(1 - \frac{a}{R} \right)^{\frac{1}{2}}; \quad (4)$$

if the interaction is non-retarded and additive, where $A_{\text{H}} = 4\pi^2 \epsilon_0 \epsilon_{\text{sw}}$ is the Hamaker constant of the system.^{31,46} (Note that in MD simulations both assumptions are implicit in using a constant interatomic potential.) The energy in this "Derjaguin approximation" exhibits limitations similar to those of the continuum description when applied at molecular scales in the case of the lubrication forces, in that the expression for V_{sw} given above diverges at contact. In fact, since the short range repulsion present in the LJ potential would prevent molecules from approaching closer than a separation distance of order σ , we could use $V_{\text{sw}}(\sigma)$ as a reasonable estimate of the energy at contact.³¹ (Note however that the snapshots in Fig. 9 show that the actual wall-sphere configuration corresponds to a more complex intermeshing of the two solids, which would be rather difficult to capture in any continuum description.)

We can correct Eq. (4) for the effect of the suspending fluid, by taking advantage of the additivity of the interatomic potential in MD simulations. Specifically, to the expression for $V_{\text{sw}}(h)$ given above, we can add a term accounting for the interaction of the tube wall with the fluid completely filling the interior of the tube, from which we then subtract the interaction of the tube wall with a sphere of fluid, located at the same position as the solid particle. The former interaction potential is a constant, independent of the position of the solid sphere and can therefore be ignored, while the latter interaction term is of the same form as Eq. (4) but multiplied by the wetting parameter A . Thus, the expression for the potential remains the same as in Eq. (4), but with an effective Hamaker constant given by $A_{\text{H}}^{\text{e}} = 4\pi^2 \epsilon_0 \epsilon_{\text{sw}} (1 - A)^2$.

The corresponding attractive force between the sphere and the tube wall is given by the derivative of Eq. (4) with respect to the separation distance h ,

$$F_{\text{sw}}(h) = -A_{\text{H}}^{\text{e}} \frac{a}{6h^2} \left(1 - \frac{a}{R} \right)^{\frac{1}{2}}; \quad (5)$$

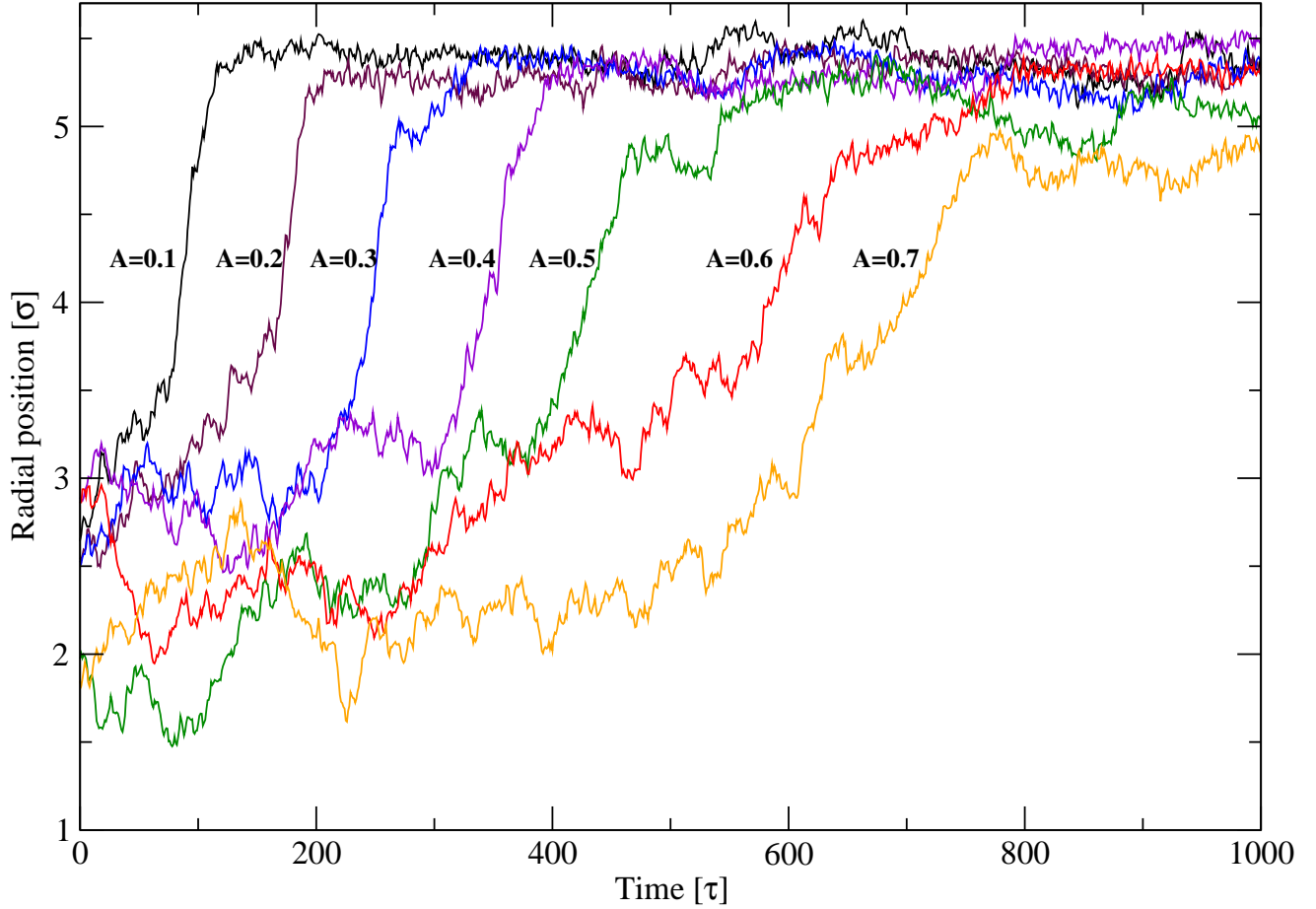


FIG. 10: Radial position of the sphere as a function of time for six single realizations to $A = 0.1, 0.2, 0.3, 0.4, 0.5, 0.6$, and 0.7 . The time axes are shifted so as to be able to observe the jump into contact in all cases. (The tube radius is $R = 6\sigma$ and the particle radius is $a = 3\sigma$.)

which is proportional to $(1 - A)$. In Fig. 10 we show that the adsorption transition strongly depends on A , in that the sudden jump into contact observed for $A = 0.1$, becomes less abrupt as the fluid becomes more wetting, and $1 - A$ decreases, which is qualitatively consistent with the previous result that the attractive force is proportional to $1 - A$.

In addition to these energetic considerations for particle adsorption, another possible mechanism, leading to attraction between solid bodies in a fluid, is a depletion force^{48,49,50,51,52} resulting from the reduction of the excluded volume and the consequent increase in the entropy when solid particles are in close proximity. However, the results given previously show that changes in the interaction energy have a dramatic effect on adsorption, and suggest that the dominant considerations are energetic as further indicated from the following "inverse" simulations. Specifically,

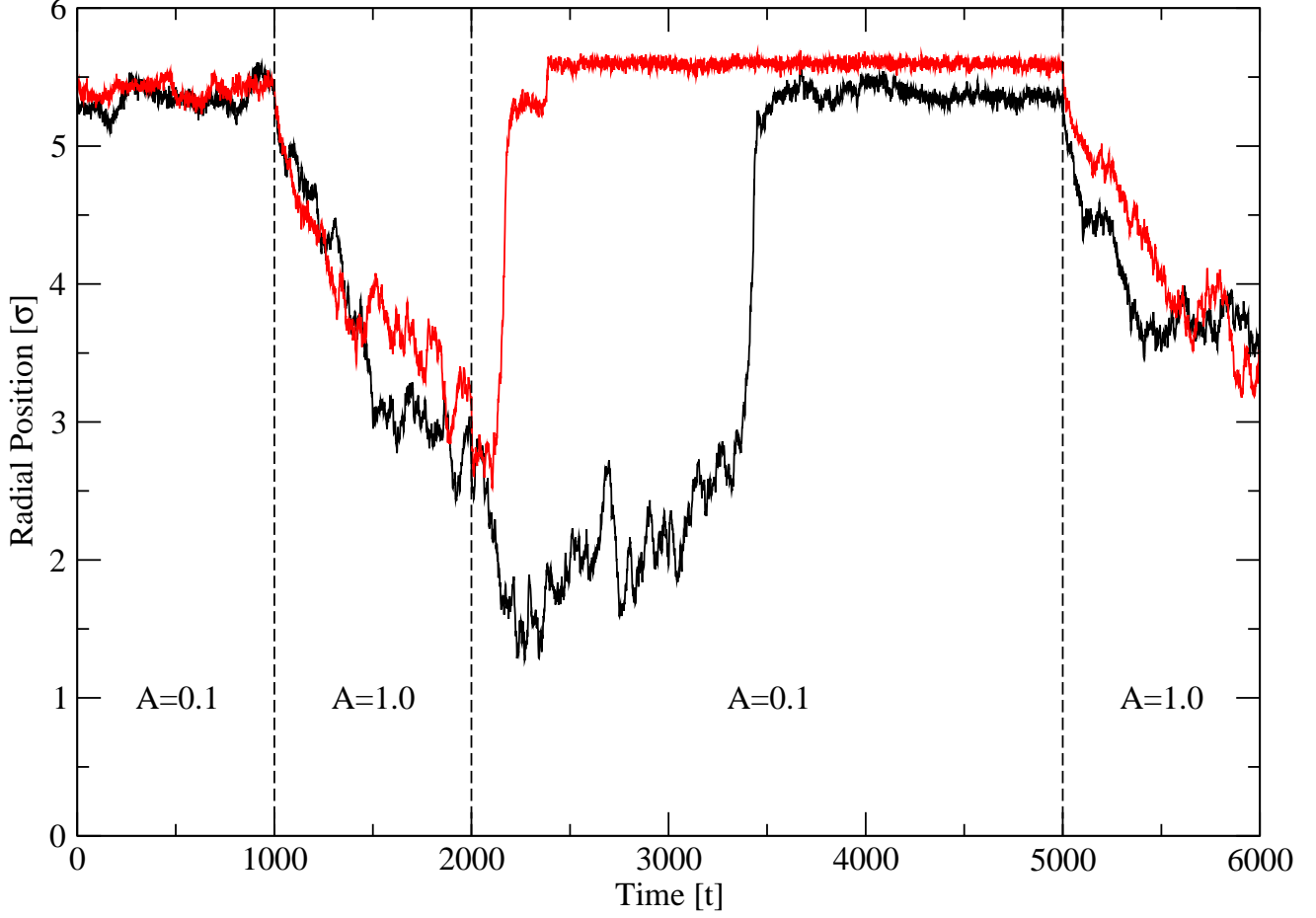


FIG. 11: Radial position of the sphere as a function of time for two independent realizations of the MD simulations. In both cases the wetting parameter is set, initially, equal to $A = 0.1$, leading to the adsorption of the particles. At $t = 1000$ the wetting parameter is changed to $A = 1.0$, and a spontaneous desorption of the spheres can be observed. After changing, at $t = 2000$, the wetting parameter back to $A = 0.1$ the spheres are re-adsorbed. (The tube radius is $R = 6\sigma$ and the particle radius is $a = 3\sigma$.)

we consider the evolution of an initially adsorbed colloidal particle suspended in a non-wetting fluid, $A = 0.1$, when the fluid is instantaneously rendered completely wetting by changing A to 1.0 . After this change, the intermolecular forces between all species are identical, so one might expect that these forces are approximately isotropic, and that only depletion forces would be available to preserve the adsorption of the particle. In Fig. 11 we present the evolution of the radial position of the sphere in two independent inverse simulations. In both cases, the wet-

ting parameter is initially set at $A = 0.1$ which, in time, leads to the sphere being adsorbed onto the tube wall; then, after allowing the sphere to equilibrate in an adsorbed position for $t = 1000$, the wetting parameter is switched to $A = 1.0$. As is seen in Fig. 11, the particles desorb spontaneously with no measurable trapping time, thereby leading us to conclude that depletion forces are not responsible for the long (perhaps irreversible) adsorption times observed in the poor wetting cases. This calculation is of course somewhat indirect in that we do not estimate directly any entropic effects, but in a forthcoming paper⁵³ we calculate the Helmholtz free energy changes associated with particle motion in nanotubes, which we hope will shed some light on this question.

Finally, we discuss the behavior of particles after adsorption. In Fig. 12 we present the radial and axial positions of a disordered sphere as it moves through a disordered tube, for the case $A = 0.2$. It is clear that, even after adsorption has taken place, the particle continues to move along the tube in the form of an intermittent stick-slip motion while remaining in near contact with the tube wall. This form of a stick-slip motion has no counterpart in any simple continuum description, because, even if it were possible for the sphere to overcome the resistance of the lubrication layer of the fluid and almost touch the cylindrical wall, say at a separation $h = a$, the force required to move it along the surface would diverge as⁵⁴ $a=h$, which far exceeds our applied force. Other types of interaction, such as double-layer effects, could lead to an equilibrium radial position of the sphere at some distance away from the wall,⁵⁵ but this also would not account for the stick-slip behavior observed here.

Stick-slip motion was found to occur for all types of ordered and disordered spheres and walls, and thus does not depend on any precise matching of their underlying molecular structures. In fact, the results shown in Fig. 12 correspond to the extreme case where the position of both the molecules of the sphere and those of the tube wall have been randomly modified. In our previous paper¹⁸ we reported that, both the average radial position of the sphere and the random fluctuations around that average, depend on whether the particle is sliding along the wall (slip) or whether it is motionless on average (stick). For the probability density function of the radial position of the solid particle, we found similar results for different types of particles and tube wall, but the distributions corresponding either to sliding or sticking particles have substantial overlap in the case of disordered solids, and the average distance to the wall in both cases is almost indistinguishable. On the other hand, in all cases there exists a strong correlation between the

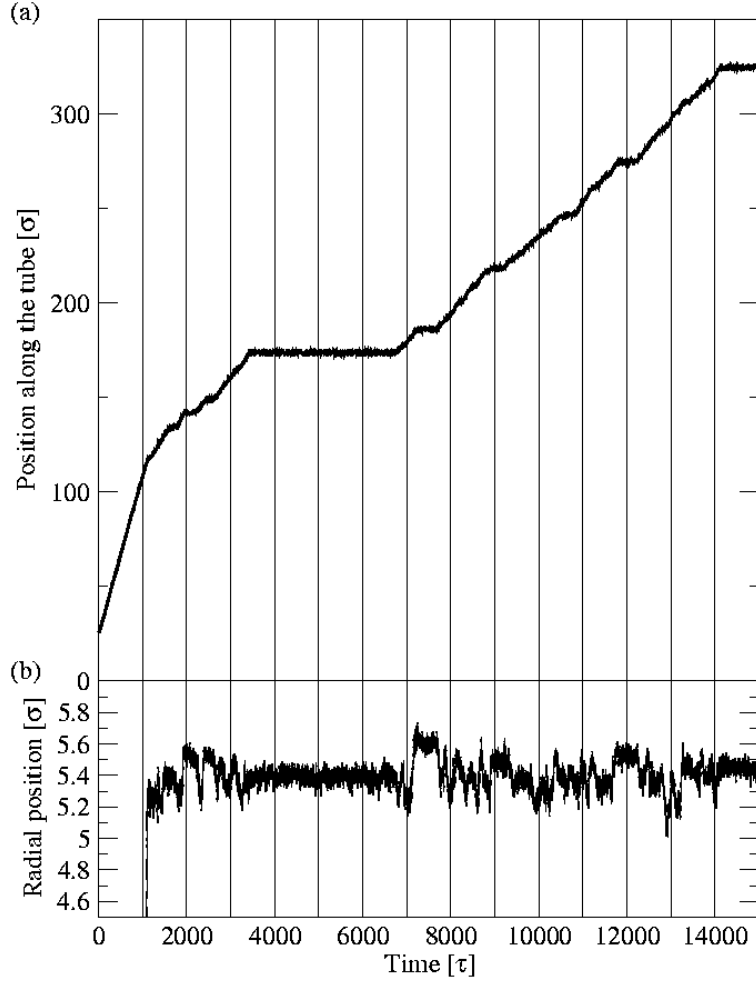


FIG. 12: (a) Position of the particle along the tube as a function of time (b) Radial position of the sphere as a function of time. The results correspond to a disordered sphere moving through a disordered tube for $A = 0.2$. (The tube radius is $R = 6$ and the particle radius is $a = 3$.)

amplitude of the fluctuations in the radial position and the motion of the particle in the axial direction. This is illustrated in Fig. 12 which shows how, during a single realization in which the particle displays intermittent stick-slip motion, the amplitude of the fluctuations in the radial position of the particle is clearly correlated to its axial motion.

VI. MOTION OF A PROLATE SPHEROID THROUGH A CYLINDRICAL CHANNEL

In practice, one may be interested in particles of more general shapes, and we now consider the motion of prolate spheroids through a cylindrical nanochannel. These spheroids were constructed in a fashion analogous to the spherical solid particles discussed in section II, with the minor axis equal to a , the radius of the spherical particles considered previously, and the major axis b related to the ellipticity e via $e = \frac{b}{a} = \frac{1}{1 - (a^2/b^2)}$. The simulations were performed for two different aspect ratios, $b/a = 3$ corresponding to $e = 0.89$ and $b/a = 5$ corresponding to $e = 0.96$, and both ordered and disordered spheroids were studied. The tube radius always equaled twice the minor radius of the spheroids, $R = 2a$, and its length was changed to $L_x = 50\lambda$ for the case of aspect ratio $b/a = 5$, in order to avoid possible hydrodynamic interactions between periodic images.

Initially the spheroids were placed at the center of the tube with their major axes oriented along the tube axis. Note that neither of the two spheroids would have fitted inside the tube if its major axis had been oriented perpendicular to the tube axis, with the maximum possible (polar) angle between the major axis of the spheroid and the tube axis being $\theta_m(b/a = 3) = 4^\circ$ and $\theta_m(b/a = 5) = 8^\circ$. As in the case of spherical particles, the surrounding fluid was first equilibrated and then a body force, linearly ramped up from zero to a final value $f = 0.1$, was applied to each atom in the spheroid. We followed the evolution of the spheroids as they moved through the tube for relatively long times, up to 10^5 to 0.25 s in some cases.

The qualitative behavior of the spheroids is very similar to that of the spheres under similar conditions. Specifically, in section V, we showed that the adsorption events are readily observable in the evolution of the radial position, as revealed by a sudden jump-into-contact of the particles. In Fig. 13 we present the time evolution of the polar angle for independent MD simulations corresponding to different wetting conditions, varying from complete wetting $A = 1.0$ to non-wetting $A = 0.1$. As in the case of the sphere, for poor wetting (low A) the polar angle suddenly locks at a certain value, a transition that corresponds to the adsorption of the spheroid, while, in the complete wetting situation, the spheroid does not adsorb even after relatively lengthy simulations. Completely analogous results are obtained for a spheroid having a larger aspect ratio, $b/a = 5$. In addition, and going beyond the observations for spherical particles, the spheroids display a certain selectivity of the orientation angles at which adsorption takes place, and this

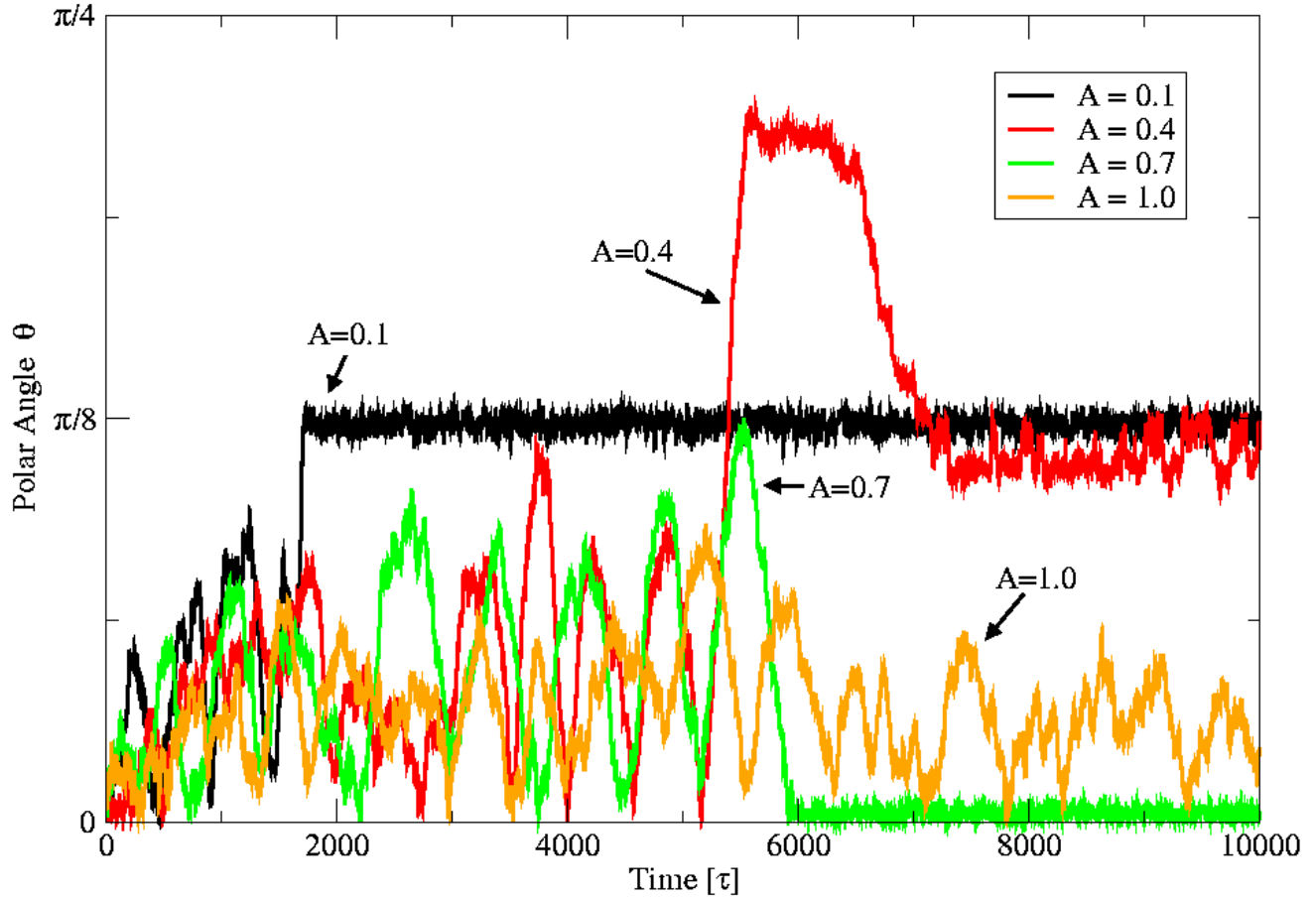


FIG. 13: Angle between the spheroid major axis and the tube axis as a function of time for four realizations at $A = 0.1, 0.4, 0.7$ and 1.0 (for each value of A one independent MD simulation is presented). The abrupt locking of the polar angle observed at $A = 0.1, 0.4$ and 0.7 corresponds to the adsorption of the spheroid on the tube wall. The tube radius is $R = 6'$. The spheroids have minor axis $a = 3'$ and aspect ratio $= 3$, and both the spheroids and the tube are ordered.

orientation remains essentially locked after adsorption. In some cases, however, a transition between two different orientations can be observed after the particle has been adsorbed (see Fig. 13 for the $A = 0.4$ case). In Fig. 14 we present the probability distribution function for the orientation of the spheroids after the occurrence of adsorption, obtained from more than 50 different realizations for spheroids with aspect ratio $= 3$, and with the wetting parameter varying from $A = 0.1$ to $A = 0.7$. We see that three different polar orientations predominate, corresponding to: i) spheroids with their major axis parallel to the tube, $\sin \theta = 0$; ii) spheroids occupying one fourth of the tube cross section $\sin \theta = R/2$; and iii) spheroids locked across the

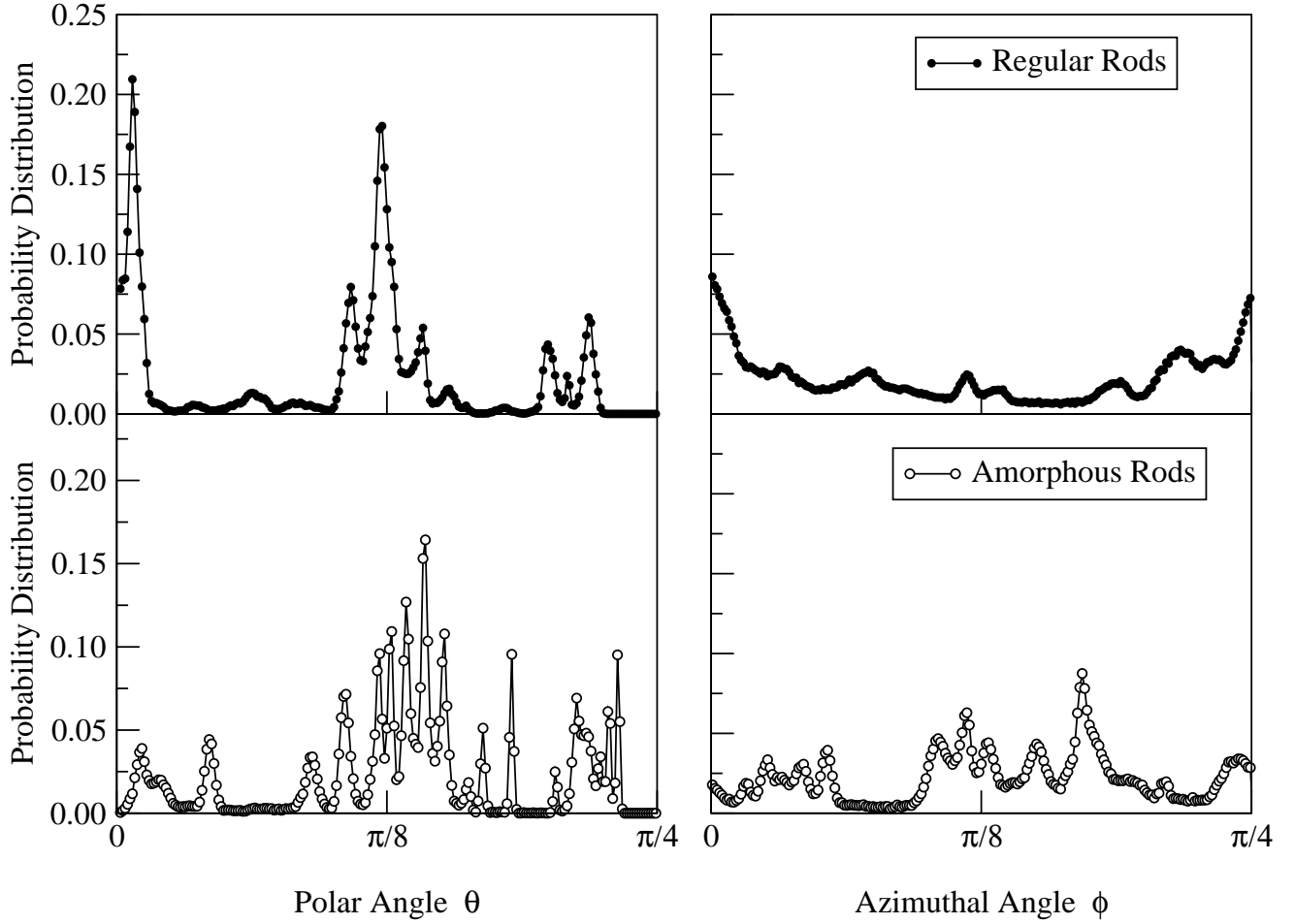


FIG. 14: Probability distribution function for the orientation angles of a spheroid after adsorption, averaged over 50 or more realizations with wetting properties ranging from $A = 0.1$ to 0.7 . The left (right) hand plots are the probability distribution functions for the polar angle (azimuthal angle), and the top (bottom) plots correspond to an ordered (disordered) spheroid and wall. The tube radius is $R = 6\sigma$. The spheroids have minor axis $a = 3\sigma$ and aspect ratio $\alpha = 3$.

tube $b \sin \theta \approx R$. Snapshots of the three possible orientations are presented in Fig. 15 for the case of disordered spheroids and a disordered tube. We can also see in this figure the complete depletion of fluid molecules from the narrowest gap between the tube wall and the spheroid.

Finally, we also observe that, after adsorption, the spheroids display, in some cases, a stick-slip motion similar to that observed for adsorbed spheres. In Fig. 16 we present the time evolution of the radial position and of the orientation for an adsorbed solid spheroid with $\alpha = 3$ and $A = 0.5$. Clearly, there exists a strong correlation between the amplitude of the fluctuations in the polar

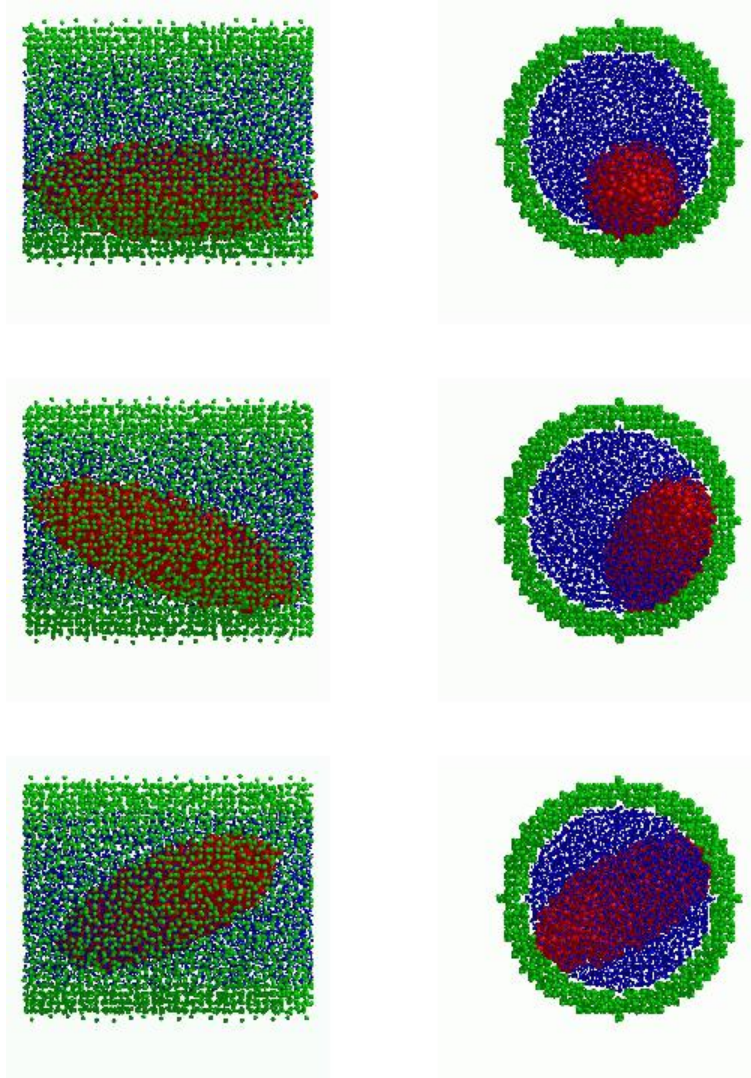


FIG .15: Three cases of spheroid adsorption in three distinct realizations for $A = 0.1$, with side views on the left and cross-sectional views on the right. The tube radius is $R = 6'$. The spheroids have minor axis $a = 3'$ and aspect ratio $\epsilon = 3$.

angle and the motion of the spheroid in the axial direction, in that, larger angular fluctuations correspond to a sliding motion, while a sticking behavior corresponds to much smaller fluctuations in the orientation.

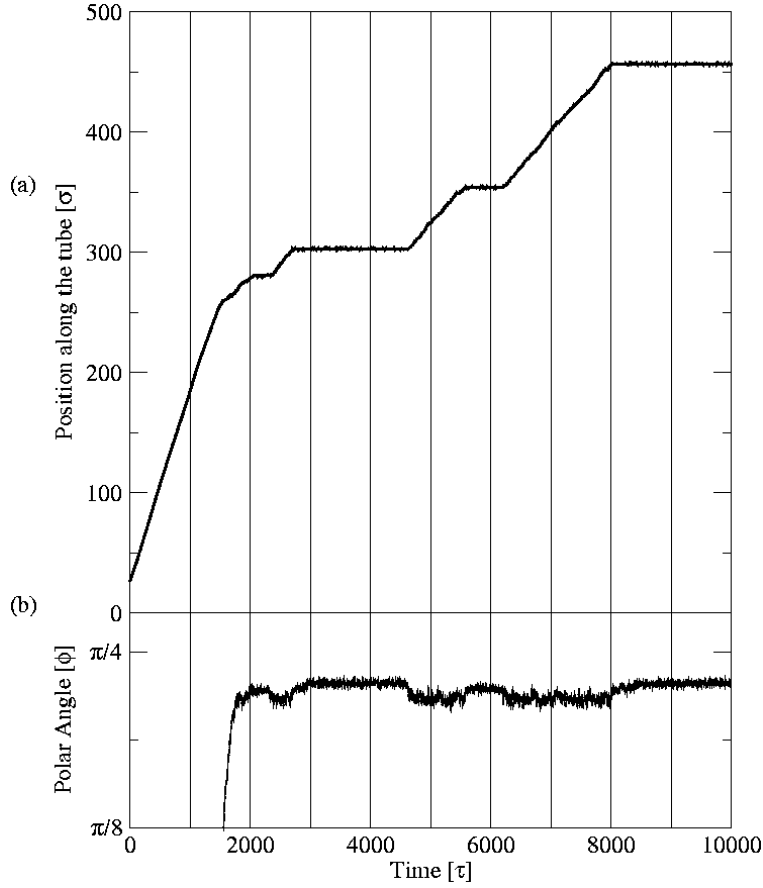


FIG. 16: (a) Position of the spheroid along the tube as a function of time, and (b) polar angle of the spheroid as a function of time, for a disordered spheroid moving through a disordered tube, for $A = 0.5$. The tube radius is $R = 6'$. The spheroids have minor axis $a = 3'$ and aspect ratio $\alpha = 3$.

VII. CRITERION FOR THE ADSORPTION TRANSITION

In the previous sections we showed that both spherical and elongated particles suspended in a poorly wetting fluid are eventually adsorbed onto the tube wall. In the simulations, the wetting properties are controlled by the parameter A in Eq. (1), and a simple estimate of the attractive force between the particle and the wall in Eq. (5) likewise involved A , so it is natural to ask whether there exists a critical value of A which identifies an adsorption transition. To this end, we simulated more than 200 cases of spheroids of aspect ratios 1, 3 or 5, in fluids with different values of A , and with either ordered or disordered atomic structures for the particle and for the tube wall, with multiple realizations in some cases.

Table II summarizes the parameters of the various runs (all with $R=a=2$). The simulations

TABLE II: Adsorption times in MD simulations. Note that an estimate of the diffusive time required to reach the tube wall by a single sphere yields $\tau_D \approx 2500$.

A	P	C	T _a	T _t	A	P	C	T _a	T _t	A	P	C	T _a	T _t	A	P	C	T _a	T _t
0.10	1		5	50	0.66	1		6	30	0.10	1	6	1.5	10	0.10	3		f3,2,3,6,3,9,3,4,5,2g	10
0.20	1		1	35	0.67	1		2	30	0.20	1	6	2.5	10	0.20	3		f3,2,2,2,1,6,9,2,3,2g	10
0.30	1		1	35	0.68	1		4	30	0.30	1	6	2	10	0.30	3		f7,2,3,2,7,6,9,3,3g	10
0.40	1		2	30	0.69	1		12	30	0.40	1	6	2.5	10	0.40	3		f-,-,3,3,6,7,5,4g	10
0.50	1		6	40	0.70	1		3	40	0.50	1	6	6	10	0.50	3		f9,5,7,5,4,3,4,5,7g	10
0.55	1		3	35	0.71	1		17	30	0.60	1	6	-	10	0.60	3		f-4,3,5,5,5,5g	10
0.60	1		6	35	0.72	1		6	30	0.70	1	6	4	10	0.70	3		f-,8,6,6,6,6,6g	10
0.65	1		8	35	0.73	1		11	30	0.80	1	6	-	10	0.80	3		f-,6,6,6,6,6,6g	10
					0.73	1		11	30	0.90	1	6	-	10	0.90	3		f-,6,6,6,6,6,6g	10
					0.74	1		5	30	1.00	1	6	-	10	1.00	3		f-,6,6,6,6,6,6g	10
					0.75	1		-	45	0.10	1	6	6	15	0.10	3	6	f2,3,2,1,1,4,3,3,3,8g	10
					0.76	1		19	40	0.20	1	6	6	15	0.30	3	6	f5,1,2,2,3,2,8,3,3g	10
					0.77	1		7	30	0.30	1	6	6	15	0.30	3	6	16	17.5
					0.78	1		9	30	0.40	1	6	6	15	0.50	3	6	f5,2,9,8,2,5,5,8g	10
					0.79	1		7	30	0.50	1	6	6	15	0.50	3	6	14	15
					0.80	1		-	35	0.60	1	6	6	15	0.50	3	6	6	12.5
					0.81	1		-	15	0.70	1	6	6	15	0.10	5		f6,3,8,6,3,7g	10
					0.82	1		-	15	0.80	1	6	6	15	0.10	5		11	12.5
					0.83	1		-	15	0.90	1	6	6	15	0.10	5		f14,14,14g	15
					0.84	1		-	15	1.00	1	6	6	15	0.30	5		f12,15,3,15,5g	17.5
					0.85	1		-	25						0.30	5		f26,27g	30
					0.86	1		-	15						0.30	5		21	22.5
					0.87	1		-	15						0.30	5		16	20
					0.88	1		-	15						0.50	5		f11,29,19,19,7g	40
					0.89	1		-	15						0.50	5		80	90
					0.90	1		-	25						0.50	5		93	100
					0.91	1		-	15						0.50	5		f-,g	110
					0.92	1		-	15						1.00	5		f-,6,6,6,6,6,6g	10
					0.93	1		-	15						0.10	5	6	f5,5g	10
					0.94	1		-	15						0.10	5	6	f7,11,5,7g	12.5
					0.95	1		-	25						0.10	5	6	15	17.5
					0.96	1		-	15						0.10	5	6	f21,22,19g	22.5
					0.97	1		-	15						0.30	5	6	f12,12,13,8g	15
					0.98	1		-	15						0.30	5	6	f19,17g	20
					0.99	1		-	15						0.30	5	6	f17,20g	25
					1.00	1		-	25						0.30	5	6	f26,27g	30

P : Particle type, O rdered; 6 D isordered.

C : Tube wall type, O rdered; 6 D isordered.

T_a : Time at which the particle is adsorbed in units of 1000 ; - means that there is no adsorption; fg list of adsorption times corresponding to multiple realizations with identical parameters and total duration.

T_t : Duration of the simulation in units of 1000 .

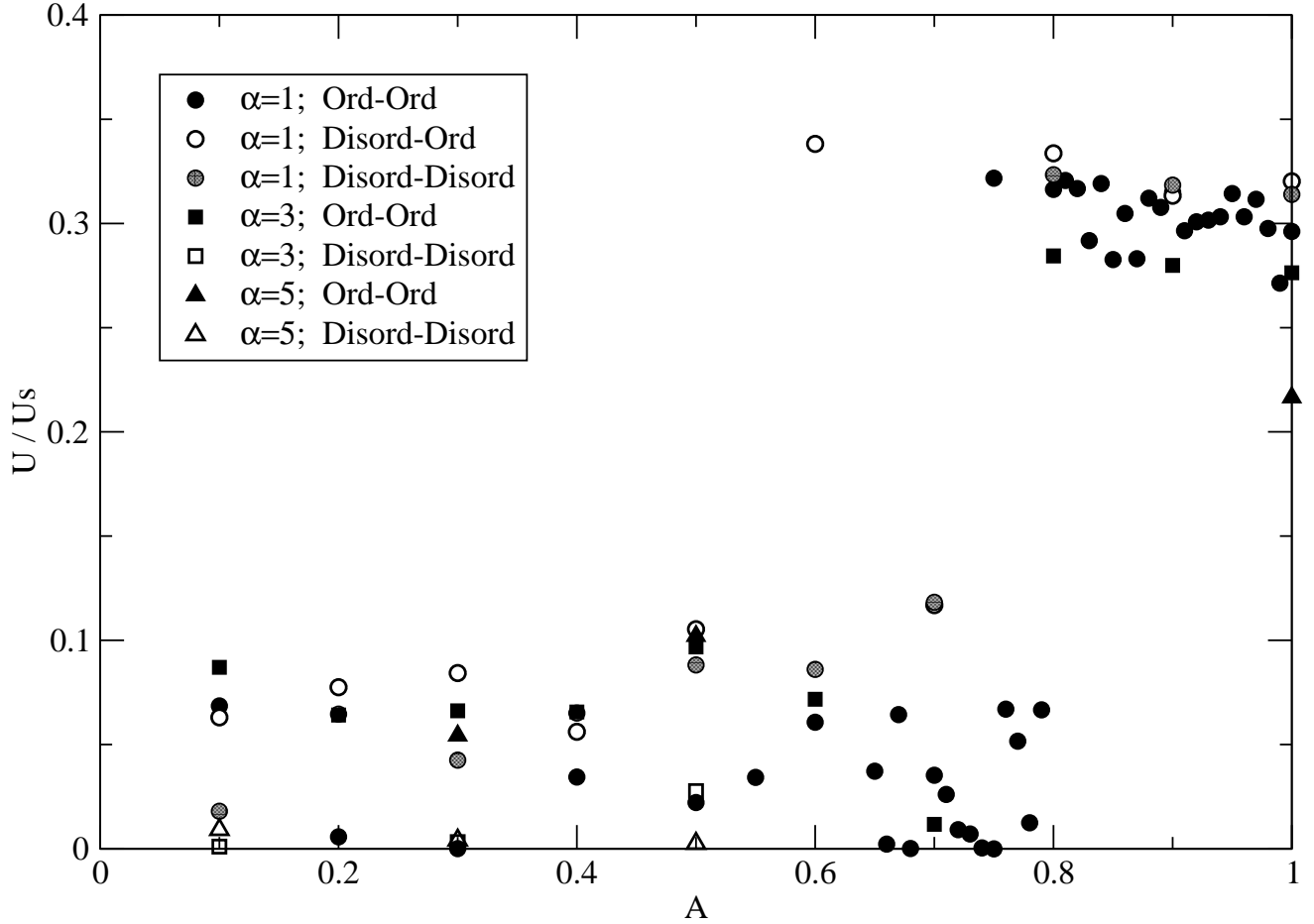


FIG. 17: Long-time average particle velocity along the tube. The velocity is normalized by the Stokes velocity U_s that a sphere having the same radius would have had in an unbounded fluid, for the same applied force and no-slip boundary conditions. The time span of the simulations, $T_t = 10000$, was always longer than the diffusive time required for the particle to reach the wall, $\tau_D = 2500$. The average velocity of particles that were adsorbed during the simulation is computed for times after adsorption had occurred, whereas, for particles that are not adsorbed the velocity is averaged over the entire simulation. The dispersion in the velocities of adsorbed particles is a consequence of the stick-slip motion after adsorption that has already been described.

ran for long times, $O(10^4)$ or longer, and we can characterize the results numerically in terms of the average particle velocity, with the result shown in Fig. 17. In this figure, the velocities are normalized by the Stokes velocity that the same particle would have had in an unbounded fluid with the same applied force,¹ $U_s(\eta) = F/(6\pi aK(\eta))$, where $K(1) = 1$, $K(3) = 1.40446$,

and $K(5) = 1.78481$. Relative velocities of 0.1 or below correspond to the stick-slip motion of adsorbed particles already described, while values near 0.3, which are similar to the velocities obtained at short times (cf. Fig. 6 at $R/a = 2$), correspond to the motion of spheres that are not adsorbed.

There exists strong evidence that the transition to adsorption occurs at $A = 0.8$ independent of particle characteristics. Moreover, we also performed additional "inverse" simulations to those discussed in Section V. We found that whereas, for $A > 0.8$, the particles are soon desorbed from the wall, for $A \leq 0.8$ the particles remained adsorbed for the duration of our simulations (e.g. 10^5 for $A = 0.6$), thus providing further evidence for the existence of a sharp transition. Since particle adsorption is a random process which requires a fluctuation to bring the particle near the wall, the time required can vary over a wide range (see table V II), and there is no guarantee that the transition to adsorption will occur during the duration of the simulation. Indeed, as is seen in Fig. 17 there is one exception to the general rule, for a sphere at $A = 0.6$.

V III. S U M M A R Y A N D C O N C L U S I O N S

The complex dynamics of suspended nanometer size particles under nano-confinement was investigated by means of molecular dynamics simulations. We studied the low Reynolds number transport of nanometer size spheroids with radius $a = 3\sigma$, and aspect ratios ranging from 1 to 5, suspended in a LJ fluid of density $\rho = 0.8$ and confined inside a nanochannel of radius ranging between $R = 4\sigma$ and $R = 12\sigma$.

We initially examined the behavior of single fluids flowing through a nanochannel for varying wetting conditions, and showed that the increase in surface-to-volume ratio, typical at the nanometer scales, changes the transport properties of the fluid in a significant way. Specifically, we showed that a change in the strength of the solid-fluid interaction leads to a small shift in the position of the first adsorbed layer of the fluid, z_{min} , which in turn leads to a relatively small increase in the fluid density at the center the tube, $\rho_{\text{center}} = 1.13\%$. This small change in density, however, has a significant effect in the corresponding fluid viscosity at the center of the tube, which shows an increase of up to 80%. However, this dependence of the viscosity on the density was shown to be in agreement with that observed in bulk fluids. The measured slip lengths are also in agreement with measurements obtained in bulk, or in substantially larger

geometries. The structure developed by the fluid close to the tube wall is also consistent with previous findings as well as with equilibrium simulations. Finally, we showed that macroscopic continuum equations that allow for slip at the solid boundaries accurately describe the velocity profile of a fully developed flow in a pipe, even in the region where the fluid is highly structured.

We then considered the motion of a spherical solid particle through a nanochannel, at both long and short times compared to the diffusive time required for the sphere to reach the wall. We first showed that, at short times, the average velocity of the particles remains essentially unaffected by changes in the wetting parameter A , particularly so for $A \geq 0.5$, and concluded that this lack of dependence on A of the mobility of the particles is due to the competition between an increase in the viscosity of the fluid and the reduction of the drag force on the particles as A decreases and the degree of wetting is reduced. Then, we compared the numerical results for the mobility of the spheres with the prediction based on continuum calculations for a non-Brownian smooth sphere moving along the centerline of a structureless tube in the limit of vanishingly small inertia. We found reasonable agreement, especially in view of the simplified continuum model that we used which does not account either for the large thermal fluctuations present in the system, or for the molecular structure of both solids. Moreover, due to the competition between drag reduction and increased viscosity as the degree of wetting is reduced, the continuum representation describes fairly well the numerical results for all wetting conditions, even though the assumed no-slip boundary condition becomes less accurate as A decreases. At long times, however, the interactions of the suspended particle with the tube wall become important and we showed, that for poorly wetting suspending fluids, $A \leq 0.8$, the particles eventually are adsorbed to the tube wall while, surprisingly, displacing all fluid atoms from the gap, and, subsequently, exhibit stick-slip motion along the tube wall. These interesting features could never have been captured by any simple continuum description, where lubrication forces would prevent the particle from either moving towards the wall or along it for small separation distances (h = λ). We then studied the contribution of van der Waals and depletion forces to the particle adsorption phenomena and concluded that the dominant contribution comes from the fluid-solid van der Waals interactions, as suggested by the dramatic effect that changes in the wetting parameter A have on the adsorption process. Simulations showing the spontaneous desorption of particles in the complete wetting situation, $A = 1.0$, confirmed the conclusion that depletion forces are weak enough to allow for the desorption of particles over extremely short times.

The behavior of prolate spheroids of two different aspect ratios, $\alpha = 3$ and $\alpha = 5$, is qualitative similar to that of the spheres, in that adsorption of the particles takes place for poor wetting conditions and that a similar stick-slip motion along the tube is also subsequently observed in some cases. In addition, spheroidal particles exhibit a certain selectivity in their final orientation upon adsorption by seemingly preferring three different orientations, two of which appear to locally maximize the contact area between the particle and the tube wall while the third appears to correspond to the dynamic locking of the spheroids across the tube section.

Finally, we investigated the adsorption transition as the wetting properties vary from non-wetting to complete wetting, and found strong evidence suggesting that the transition occurs at $\alpha \approx 0.8$ independent of particle shape. A detailed study of the Helmholtz free energy of the system for different wetting conditions is currently being performed and will be the topic of a forthcoming paper.⁵³

Acknowledgements

G.D. thanks J. Halverson for carefully reading the manuscript and for helpful comments. This work was supported by the Engineering Research Program, Office of Basic Energy Sciences, U.S. Department of Energy under Grant DE-FG 02-03ER 46068.

Electronic address: drazer@mailaps.org

- ¹ J. Happel and H. Brenner, *Low Reynolds Number Hydrodynamics* (Prentice-Hall, New Jersey, 1965).
- ² J. Koplik and J.R. Banavar, *Ann. Rev. Fluid Mech.* **27**, 257 (1995).
- ³ J. Koplik, J.R. Banavar, and J.F. Willemsen, *Phys. Fluids A* **1**, 781 (1989).
- ⁴ P.A. Thompson and M.O. Robbins, *Phys. Rev. Lett.* **63**, 766 (1989).
- ⁵ H.A. Stone, A.D. Stroock, and A. Ajdari, *Annu. Rev. Fluid Mech.* **36**, 381 (2004).
- ⁶ D.R. Reyes, D. Iossidis, P.A. Auroux, and A. Manz, *Analytical Chemistry* **74**, 2623 (2002).
- ⁷ P.A. Auroux, D. Iossidis, D.R. Reyes, and A. Manz, *Analytical Chemistry* **74**, 2637 (2002).
- ⁸ P. Gravesen, J. Branebjerg, and O.S. Jensen, *J. Micromech. Microeng.* **3**, 168 (1993).
- ⁹ C.M. Ho and Y.C. Tai, *Annu. Rev. Fluid Mech.* **30**, 579 (1998).
- ¹⁰ N. Giordano and J.T. Cheng, *J. Phys. Cond. Mat.* **13**, R271 (2001).

- ¹¹ H . A . Stone and S . K im , *A i c h e J.* 47 , 1250 (2001).
- ¹² S . R . Q u a k e and A . S c h e r e r , *Science* 290 , 1536 (2000).
- ¹³ C . L e e , E . H . Y a n g , N . V . M y u n g , and T . G e o r g e , *N a n o L e t t e r s* 3 , 1339 (2003).
- ¹⁴ J . W . H o n g and S . R . Q u a k e , *N a t u r e B i o t e c h n o l o g y* 21 , 1179 (2003).
- ¹⁵ G . H u m m e r , J . C . R a s a i a h , and J . P . N o w o r y t a , 414 pp. 188{190 (2001).
- ¹⁶ H . G r u b m u l l e r , *P r o c . N a t . A c a d . S c i.* 100 , 7421 (2003).
- ¹⁷ O . B e c k s t e i n and M . S . P . S a n s o m , *P r o c . N a t . A c a d . S c i.* 100 , 7063 (2003).
- ¹⁸ G . D r a z e r , J . K o p l i k , A . A c r i v o s , and B . K h u s i d , *P h y s . R e v . L e t t.* 89 , 244501 (2002).
- ¹⁹ M . P . A l l e n and D . J . T i l d e s l e y , *C o m p u t e r S i m u l a t i o n o f L i q u i d s* (C l a r e n d o n P r e s s , O x f o r d , 1987).
- ²⁰ W . G . H o o v e r , *P h y s . R e v . A* 31 , 1695 (1985).
- ²¹ H . G o l d s t e i n , *C l a s s i c a l M e c h a n i c s* (A d d i s o n - W e s l e y , M a s s a c h u s e t t s , 1987).
- ²² J . R . E r r i n g t o n , P . G . D e b e n e d e t t i , and S . T o r q u a t o , *J . C h e m . P h y s.* 118 , 2256 (2003).
- ²³ J . L . B a r r a t and L . B o c q u e t , *P h y s . R e v . L e t t.* 82 , 4671 (1999).
- ²⁴ J . L . B a r r a t and L . B o c q u e t , *F a r a d a y D i s c u s s.* 112 , 119 (1999).
- ²⁵ P . G . d e G e n n e s , *R e v . M o d . P h y s.* 57 , 827 (1985).
- ²⁶ J . R o w l i n s o n and B . W i d o m , *M o l e c u l a r t h e o r y o f c a p i l l a r i t y* (C l a r e n d o n P r e s s , O x f o r d , U K , 1982), 2nd ed.
- ²⁷ M . C i e p l a k , J . K o p l i k , and J . R . B a n a v a r , *P h y s i c a A* 287 , 153 (2000).
- ²⁸ S . E . D o n n e l l y , R . C . B i r t c h e r , C . W . A l l e n , I . M o r r i s o n , K . F u r u y a , S . M i n g h u i , K . M i t s u i s h i , and U . D a h m e n , *Science* 296 , 507 (2002).
- ²⁹ P . A . T h o m p s o n and M . O . R o b b i n s , *P h y s . R e v . A* 41 , 6830 (1990).
- ³⁰ J . K o p l i k , J . R . B a n a v a r , and J . F . W i l l e m s e n , *P h y s . R e v . L e t t.* 60 , 1282 (1988).
- ³¹ J . I s r a e l a c h v i l i , *I n t e r m o l e c u l a r & S u r f a c e F o r c e s* (A c a d e m i c P r e s s , 1991).
- ³² I . B i t s a n i s , J . J . M a g d a , M . T i r r e l l , and H . T . D a v i s , *J . C h e m . P h y s.* 87 , 1733 (1987).
- ³³ D . M . H e y e s , *P h y s . R e v . B* 37 , 5677 (1988).
- ³⁴ W . T . A s h u r s t and W . G . H o o v e r , *P h y s . R e v . A* 11 , 658 (1975).
- ³⁵ R . B . B i r d , W . E . S t e w a r t , and E . N . L i g h t f o o t , *T r a n s p o r t P h e n o m e n a* (W i l e y T e x t B o o k s , N e w Y o r k , 2001), 2nd ed.
- ³⁶ M . C i e p l a k , J . K o p l i k , and J . R . B a n a v a r , *P h y s . R e v . L e t t.* 86 , 803 (2001).
- ³⁷ U . H e i n b u c h and J . F i s c h e r , *P h y s . R e v . A* 40 , 1144 (1989).

- ³⁸ N . Liron and R . Shabar, J. Fluid Mech. 86, 727 (1978).
- ³⁹ H . Wang and R . Skalak, J. Fluid Mech. 38, 75 (1969).
- ⁴⁰ B . X . Cui, H . Diamant, and B . H . Lin, Phys. Rev. Lett. 89, 188302 (2002).
- ⁴¹ P . M . Bungay and H . Brenner, Int. J. Multiphase Flow 1, 25 (1973).
- ⁴² M . Vergeles, P . Koblinski, J . Koplek, and J . R . Banavar, Phys. Rev. Lett. 75, 232 (1995).
- ⁴³ M . Vergeles, P . Koblinski, J . Koplek, and J . R . Banavar, Phys. Rev. E 53, 4852 (1996).
- ⁴⁴ N . Sushko and M . Cieplak, Phys. Rev. E 64, 021601 (2001).
- ⁴⁵ P . M . Bungay and H . Brenner, J. Fluid Mech. 60, 81 (1973).
- ⁴⁶ W . B . Russel, D . A . Saville, and W . R . Schowalter, Colloidal dispersions (Cambridge University Press, Cambridge, UK, 1989).
- ⁴⁷ V . A . Kirsch, Adv. Coll. Int. Sci. 104, 311 (2003).
- ⁴⁸ P . D . Kaplan, J . L . Rouke, A . G . Yodh, and D . J . Pine, Phys. Rev. Lett. 72, 582 (1994).
- ⁴⁹ P . D . Kaplan, L . P . Faucheux, and A . J . Libchaber, Phys. Rev. Lett. 73, 2793 (1994).
- ⁵⁰ A . D . Dinsmore, A . G . Yodh, and D . J . Pine, Nature 383, 239 (1996).
- ⁵¹ Y . N . Ohshima, H . Sakagami, K . Okumoto, A . Tokoyoda, T . Igarashi, K . B . Shintaku, S . . Toride, H . . Sekino, K . . Kabuto, and I . . Nishio, Phys. Rev. Lett. 78, 3963 (1997).
- ⁵² A . D . Dinsmore, D . T . Wong, P . Nelson, and A . G . Yodh, Phys. Rev. Lett. 80, 409 (1998).
- ⁵³ In preparation.
- ⁵⁴ J . J . L . Higdon and G . P . M ucklowney, J. Fluid Mech. 298, 193 (1995).
- ⁵⁵ P . M . Adler, Physicochem . Hydrodyn. 4, 1 (1983).